(2)

EXPERIMENTAL SIMULATION OF TRANSONIC VORTEX-AIRFOIL INTERACTIONS

FINAL REPORT

Donald R. Wilson and Donald D. Seath

October 31, 1988

U.S. Army Research Office

Grant DAAG29-84-K-0131

The University of Texas at Arlington

Approved for Public Release;
Distribution Unlimited

UNCLASSIFIED
SECURITY CLASSIFICATION OF THIS PAGE (When Data Entered)

MASTER COPY - FOR REPRODUCTION PURPOSES

REPORT DOCUMENTATION PAGE

READ INSTRUCTIONS BEFORE COMPLETING FORM

1. REPORT NUMBER: ARO 21346.4-EG	2. GOVT ACCESSION NO.: N/A
3. RECIPIENT'S CATALOG NUMBER: N/A	
4. TITLE (and Subtitle): Experimental Simulation of Transonic Vortex-Airfoil Interactions	5. TYPE OF REPORT & PERIOD COVERED: Final Report, Aug. 1, 1984- Aug. 31, 1988
	6. PERFORMING ORG. REPORT NUMBER:
7. AUTHOR(s): Donald R. Wilson and Donald D. Seath	8. CONTRACT OR GRANT NUMBER(s): DAAG29-84-K-0131
9. PERFORMING ORGANIZATION NAME AND ADDRESS: The University of Texas at Arlington, Arlington, TX 76019	10. PROGRAM ELEMENT, PROJECT, TASK AREA & WORK UNIT NUMBERS:
11. CONTROLLING OFFICE NAME AND ADDRESS: U. S. Army Research Office, Post Office Box 12211, Research Triangle Park, NC 27709	12. REPORT DATE: October 31, 1988
	13. NUMBER OF PAGES: 47
14. MONITORING AGENCY NAME & ADDRESS (if different from Controlling Office):	15. SECURITY CLASS. (of this report): Unclassified
	15a. DECLASSIFICATION/DOWNGRADING SCHEDULE:

16. DISTRIBUTION STATEMENT (of this Report)

Approved for public release; distribution unlimited.

17. DISTRIBUTION STATEMENT (of the abstract entered in Block 20, if different from Report)

NA

18. SUPPLEMENTARY NOTES

The view, opinions, and/or findings contained in this report are those of the author(s) and should not be construed as an official Department of the Army position, policy, or decision, unless so designated by other documentation.

19. KEY WORDS (Continue on reverse side if necessary and identify by block number)

Blade-Vortex Interaction (BVI)
Transonic Aerodynamics
Ludwieg-tube Transonic Wind Tunnel

20. ABSTRACT (Continue on reverse side if necessary and identify by block number)

Results from an experimental investigation of helicopter rotor blade-vortex interaction (BVI) phenomena at transonic Mach numbers and at Reynolds numbers representative of actual helicopter flight operations are presented. The study examined both perpendicular (vortex core perpendicular to the blade leading edge) and parallel (vortex core parallel to blade leading edge) interaction geometries. The tests were conducted in UTA's Transonic, High-Reynolds Number, Ludwieg-Tube Wind Tunnel. Supporting tests were also conducted in the low-speed wind tunnel.

DD FORM 1 JAN 73 1473 EDITION OF 1 NOV 65 IS OBSOLETE

UNCLASSIFIED
SECURITY CLASSIFICATION OF THIS PAGE (When Data Entered)

The significant results of the investigation are summarized separately for the perpendicular and the parallel interaction:

1. Perpendicular Interaction: The effect of the vortex causes a large reduction in upper surface pressure distribution (lift increase). This lift increase correlates with strength of the vortex and closeness of the vortex encounter. The interaction is most pronounced near the leading edge of the airfoil. A large spanwise deflection of the vortex is observed as it passes over the airfoil.

2. Parallel Interaction: A similar reduction in upper surface pressure distribution is also observed during the transient passage of the parallel vortex over the airfoil. Like the perpendicular interaction, this effect is also most pronounced near the leading edge, which is in contrast to the general results of numerous CFD simulations. For certain combinations of vortex strength and encounter distance, a class-C shock motion (forward propagation of the airfoil shock wave) was observed.

In general, the results for the transonic and low-speed tests were qualitatively similar, with the principal differences attributed to vortex-shock wave interactions.

EXPERIMENTAL SIMULATION OF TRANSONIC VORTEX-AIRFOIL INTERACTIONS

FINAL REPORT

Donald R. Wilson and Donald D. Seath

October 31, 1988

U.S. Army Research Office

Grant DAAG29-84-K-0131

The University of Texas at Arlington

Approved for Public Release;
Distribution Unlimited

THE VIEW, OPINIONS, AND/OR FINDINGS CONTAINED IN THIS REPORT ARE THOSE OF THE AUTHOR(S) AND SHOULD NOT BE CONSTRUED AS AN OFFICIAL DEPARTMENT OF THE ARMY POSITION, POLICY, OR DECISION, UNLESS SO DESIGNATED BY OTHER DOCUMENTATION.

TABLE OF CONTENTS

1.0 STATEMENT OF THE PROBLEM

The primary objective of the research program supported by this grant was the experimental investigation of helicopter rotor blade-vortex interaction (BVI) phenomena at transonic blade Mach numbers, and at Reynolds numbers representative of actual helicopter flight operations. This study included an investigation of both the perpendicular (vortex core perpendicular to the blade leading edge) and parallel (vortex core parallel to the blade leading edge) interaction geometries. The tests were conducted in UTA's Transonic, High-Reynolds Number, Ludwieg-Tube Wind Tunnel (Ref. 1). Supporting tests were also conducted in UTA's Low Speed Wind Tunnel (Ref. 1).

Principal test variables included Mach number, Reynolds number, vortex strength, vortex-airfoil interaction geometry, and height of the vortex core above the test airfoil. The experimental characterization of the BVI interaction included detailed probing of the vortex structure (total pressure rake and 5-hole probe surveys), airfoil surface pressure distributions, smoke-flow visualization (low-speed wind tunnel) and holographic interferometry (transonic wind tunnel). The holographic interferometry study was initiated as part of this grant program and subsequently transferred to a second ARO grant (DAAL03-86-K-0149) that is still in progress.

2.0 SUMMARY OF RESULTS

As stated in Section 1.0, the investigation of both the perpendicular and parallel blade-vortex interactions was conducted in the low speed wind tunnel as well as the transonic Ludwieg-tube wind tunnel. The perpendicular interaction is essentially a three-dimensional steady-flow phenomenon, whereas the parallel interaction is a two-dimensional transient-flow phenomenon. The geometries are illustrated in Fig. 2.1. The perpendicular interaction was simulated by using a semi-span vortex generator wing located at the entrance to the test section and pitched to a pre-set angle of attack to generate a tip vortex that trailed downstream to interact with an instrumented test airfoil. For the simulation of the parallel interaction, a full-span vortex generator airfoil was located at the entrance to the test section, and impulsively-pitched to a pre-selected angle of attack after stabilization of the tunnel flow to shed a starting vortex that convects downstream past an instrumented test airfoil.

A summary of the significant results of the investigation is presented in the following sections for both the low-speed and transonic wind tunnel test programs. Copies of the individual conference papers and journal publications are included in Appendix A.

2.1 Low-Speed Wind Tunnel: Perpendicular Interaction

The principal results of the low-speed vortex-airfoil interaction tests are presented in Ref. 2, that is reproduced in the Appendix.

The low-speed tunnel tests were conducted using a pressure-tapped wing model that spanned the test section and located downstream of a half-wing model that generated a tip vortex. Tests of this perpendicular vortex-airfoil interaction showed that the vortex caused a substantial change in the pressure distribution of the downstream wing. The effect of the vortex on the airfoil pressure distribution was most-pronounced near the leading edge of the airfoil. The vortex also exhibited

a spanwise drift as it passed over the wing. The spanwise drift was in the same direction as the spanwise component of the induced flow at the wing surface, and may be attributed to an image effect, similar to the drifting apart of a wing's trailing vortices as they approach the ground.

In order to calculate the observed spanwise drift of a vortex during a perpendicular vortex-airfoil interaction in the low-speed wind tunnel, a simple calculation scheme was formulated and reported in Ref. 3. A copy is included in the Appendix. The scheme was based on the lifting-line solution of a wing's spanwise load distribution, as influenced by the interacting vortex, with the bound vorticity distributed along the chord in accordance with thin airfoil theory.

The resulting vortex drift calculations were in good agreement with experimental results for vortices which were not too close to the airfoil surface. The drift of a close-in vortex was substantially affected by its viscous core, a feature not included in the calculation scheme.

2.2 Low-Speed Wind Tunnel: Parallel Interaction

Low-speed wind tunnel tests were conducted to investigate the parallel blade-vortex interaction and reported in Refs. 4-5. Flow visualization tests of vortex generation performed prior to the pressure tests showed that a well defined starting vortex was generated by an impulsively pitched wing. Time history of the pressure distribution on a pressure-tapped wing model was acquired as the starting vortex passed over the wing. These pressure tests revealed that a substantial pressure change near the leading edge was induced by the encountering vortex. The effects of vortex proximity, reduced frequency and maximum pitch angle of the vortex generator on the pressure change were also investigated.

Further tests were conducted to determine the damping effects of the 3-foot long, 1/16-in diameter tube between static pressure ports and the pressure transducer. A smaller transducer was placed inside the airfoil, reducing the tube

length to approximately six inches and many of the tests were rerun. As expected, the results showed that the magnitude of pressure changes had been damped (in the original tests) by as much as a factor of two. Also, secondary smaller pressure variations, perhaps due to generation of multiple parallel vortices, were detected with the shortened tube length. However, all qualitative features of the original BVI tests remain unchanged.

2.3 Transonic Wind Tunnel: Perpendicular Interaction

The perpendicular blade-vortex interaction was simulated in UTA's high-Reynolds number, transonic, Ludwieg-tube wind tunnel (Refs. 1,6). The specific objectives of this phase of the investigation were to first develop the capability of performing blade-vortex interaction experiments in short-duration test facilities, and then to quantify the effects of Mach number, Reynolds number, vortex strength, and interaction geometry on the perpendicular blade-vortex interaction. The Mach number range of the tests was from 0.68 to 0.86, with chord Reynolds numbers varying from 3.8 to 5.5 million. Details of the investigation are reported in Refs. 7-8, and a brief summary of the significant results is presented below.

1. Use of the Ludwieg-tube facility proved to be quite adequate for simulating the perpendicular blade-vortex interaction at transonic Mach numbers and realistic flight Reynolds numbers. Tuning of the starting valve timing sequence resulted in steady-flow testing times of about 120 msec, which proved more than adequate with the existing data acquisition system (1 msec data scanning interval). The vortex surveys required repeated tunnel firings at the same test conditions in order to map the vortex structure, however, repeatability tests indicated that run-to-run variations of test conditions were minimal.

   Extensive tests were run to verify the accuracy of the Ludwieg-tube tunnel in duplicating published data on surface pressure distributions for the NACA-0012 airfoil used in the BVI study. The resulting agreement was excellent at

subcritical and low supercritical Mach numbers, however at higher supercritical Mach numbers ($M_0 > .8$), slight surface irregularities associated with the procedure used for installation of the pressure taps caused the shock to occur at a more forward chord station than indicated by data from larger tunnels. This limited the confidence level in the results at the higher free-stream Mach numbers.

2. The trailing tip vortex proved to be quite intense, with total pressure deficits in the viscous core of the order of 25 percent of the free-stream total pressure. A 5-hole probe survey indicated that the vortex possessed a well-defined viscous core ($d/c \cong 0.25$). The total pressure as well as the 5-hole probe surveys indicated a high-frequency fluctuation of pressure within the core of the vortex, with total pressure fluctuations on the order of 10 to 15 percent of the free-stream total pressure, and a frequency of at least 1 kHz. These fluctuations are thought to be a result of a high-frequency meandering of the vortex core. Time averaging of the transient pressure measurement yields a steady, repeatable time-mean pressure contour map.
3. The interaction of the vortex with the trailing airfoil results in a span-wise deflection of the vortex core as it passes over the airfoil. The trend was qualitatively similar to that observed for the low-speed tunnel test, although the magnitude of the span-wise deflection was considerably larger at transonic conditions ($s/c_{max} \cong 0.42$ compared to $s/c_{max} \cong 0.16$ for the low-speed test).
4. The interaction of the tip vortex with the trailing airfoil also results in a significant change in the airfoil surface pressure distribution. Again the results were qualitatively similar to those observed in the low-speed wind tunnel, with the predominant effect occurring near the airfoil leading edge. The increase in the peak (negative) pressure coefficient correlated with vortex strength and height of the vortex core above the airfoil surface. Integrated

upper surface pressure coefficients indicated a peak $\Delta\overline{C}p$ of about 40 percent for the case of the strongest vortex and closest encounter.

2.4 Transonic Wind Tunnel: Parallel Interaction

The objectives of this test program were similar to those described in Section 2.3; the primary difference being the change in interaction geometry and method of generating the vortex. Detailed results will be presented in Ref. 9, which is being prepared for submission to the AIAA 20th Fluid Dynamics, Plasma Dynamics and Lasers Conference. A copy of the abstract is included in the Appendix.

The transonic flow investigation consisted of three distinct sets of experiments:

1) Development of the technique of generating a starting vortex by impulsively pitching a full-span NACA 0012 airfoil section to a pre-set angle of attack after stabilization of the tunnel flow. Maximum pitch rates of 14 rad/sec were obtained, which correspond to reduced frequencies of about .003. A total pressure rake containing five high-response Kulite model XQ-093-50 probe transducers was located downstream of the pitching airfoil to characterize the transient pressure fluctuations associated with generation and shedding of the starting vortex. Supporting CFD simulations of the vortex shedding associated with the impulsive pitch maneuver were carried out by Dr. Henry Jones at NASA-Langley Research Center to aid in the qualitative interpretation of the flow structure, and will be incorporated into Ref. 9.

2) Dynamic calibration of an instrumented NACA 0012 airfoil in the transonic wind tunnel. The airfoil contained eight (8) fast-response, surface-mounted Kulite model LQ-080-100 pressure transducers. These were located from the 10 percent to 80 percent chord station (10 percent intervals). Small surface irregularities associated with the transducer installation (particularly in the high-curvature region near the leading edge of the airfoil) resulted in a departure of the base-line pressure distribution from established NACA 0012 data. Therefore, the results

presented for the subsequent BVI experiments are focussed on explanation of the departure of the pressure distribution from the base-line distribution due to passage of the vortex.

3) Simulation of the parallel BVI encounter in the transonic wind tunnel at Mach numbers ranging from 0.7 to 0.85, and airfoil chord Reynolds numbers of 3.5-5.5 million. The experimental results indicate a substantial change in pressure distribution over the leading 30 percent of the airfoil, with noticeably reduced effect over the trailing region of the airfoil. Again, this is qualitatively similar to the results observed in the low-speed tests, and also in agreement with the results presented by Caradonna (Ref. 9). This is in sharp contrast to the conclusions of Srinivasan, et. al (Ref. 10) and Jones (Ref. 11) that were based on CFD simulations of the parallel blade-vortex interaction. Their results suggested a more-uniform level of interaction over the entire chord-wise extent. Experimental data for supercritical Mach numbers suggests a very strong interaction of the vortex and the airfoil upper surface shock wave, and at closer encounters, these interactions cause an unsteady flow separation of the leading 40 percent of the airfoil chord. Experiments with stronger vortices at supercritical Mach numbers result in a forward propagation of the airfoil shock wave.

2.5 Holographic Interferometry Using Photorefractive Crystals as the Recording Media

The research into holographic interferometry was initiated to provide qualitative flow visualization to support the interpretation of aerodynamic data taken in the Ludwieg-tube transonic wind tunnel. The unique feature of the system that was developed involves the use of photorefractive crystals as the recording media, rather than photographic film. This permits the use of volumetric storage via angular multiplexing, the ability to work in ordinary laboratory environments without darkroom requirements, direct data transfer of

the recorded holograms into a digitizing camera for improved data processing and the future promise of dynamic holography. This research effort was initiated as part of this grant, and subsequently transferred to another ARO Grant (DAAL03-86-K-0149) that is still in progress. The system has been installed in the transonic Ludwieg-tube wind tunnel facility, and research is currently in progress to provide qualitative interpretation to the various blade-vortex interaction flow fields that were previously investigated with standard aerodynamic diagnostic techniques. The results of this investigation will be presented in a subsequent publication.

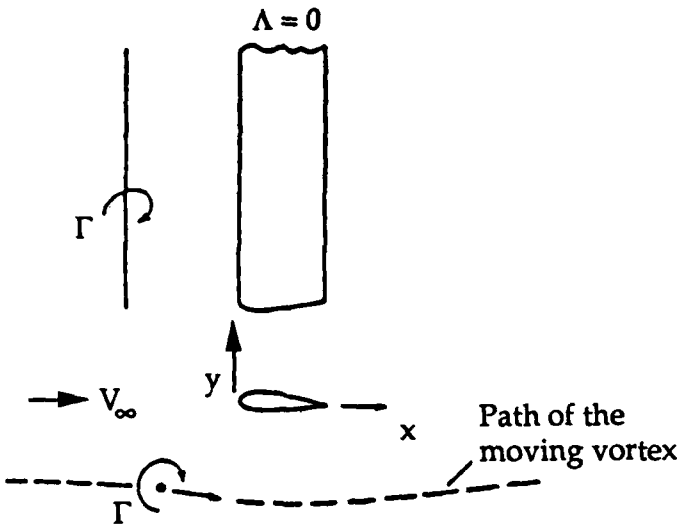

(a) Vortex parallel to leading edge

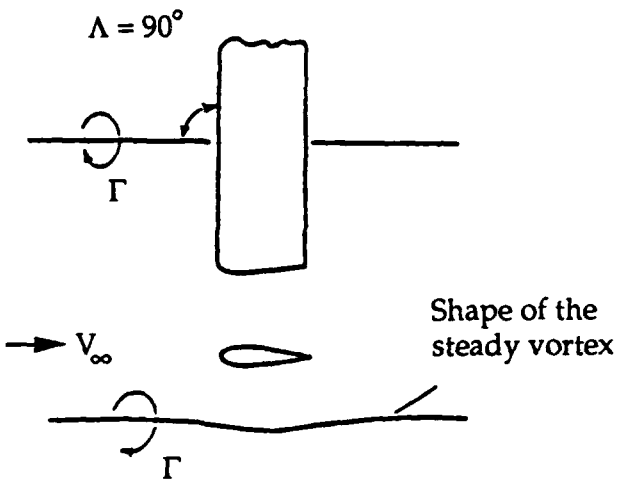

(b) Vortex parallel to free stream

Figure 2.1 Parallel and Perpendicular Blade-Vortex Interactions

3.0 PUBLICATIONS

The following conference papers, theses and journal articles were published to document the results of the research program.

1. Wilson, D. R. and Seath, D. D., "Experimental Simulation of Transonic Vortex-Airfoil Interactions," ARO Workshop on Blade-Vortex Interactions, NASA Ames Research Center, CA, October 27-31, 1984.

2. Seath, D. D. and Wilson, D. R., "Vortex-Airfoil Interaction Tests," AIAA Paper 86-0354, AIAA 24th Aerospace Sciences Meeting, Reno, Nevada, Jan. 6-9, 1986.

3. Kim, J. M., "An Investigation of the Parallel Blade Vortex Interaction in a Low Speed Wind Tunnel," M.S. Thesis, The University of Texas at Arlington, May 1986.

4. Wang, H. S., "The Perpendicular Vortex-Airfoil Interaction," M.S. Thesis, The University of Texas at Arlington, August 1986.

5. Wilson, D. R., Kalkhoran, I. M. and Seath, D. D., "An Experimental Investigation of the Perpendicular Vortex-Airfoil Interaction at Transonic Speeds,"AIAA Paper 87-0208, AIAA 25th Aerospace Sciences Meeting, Reno, Nevada, January 12-15, 1987.

6. Seath, D. D., Kim, J. M. and Wilson, D. R., "An Investigation of the Parallel Blade-Vortex Interaction in a Low-Speed Wind Tunnel," AIAA Paper 87-1345, AIAA 19th Fluid Dynamics, Plasma Dynamics and Lasers Conference, Honolulu, Hawaii, June 8-10, 1987.

7. Bhargava, A. V., "Design and Calibration of Strain Gage Balance," M.S. Thesis, The University of Texas at Arlington, August 1987.

8. Kalkhoran, I. M., "An Experimental Investigation of the Perpendicular Vortex-Airfoil Interaction at Transonic Speeds," Ph.D. Dissertation, The University of Texas at Arlington, December 1987.

9. Jung, Y. and Seath, D. D., "Spanwise Displacement of a Line Vortex Above a Wing - A Simple Calculation Scheme," AIAA Journal of Aircraft, Vol. 25, No. 5, May 1988, pp. 476-478.

10. Jung, Y., "A Solution Procedure for Incompressible Navier-Stokes Equations," Ph.D. Dissertation, The University of Texas at Arlington, August 1988.

11. Seath, D. D., Kim, J. M. and Wilson, D. R., "An Investigation of the Parallel Blade-Vortex Interaction in a Low-Speed Wind Tunnel." Accepted for publication, AIAA Journal of Aircraft.

12. Kalkhoran, I. M. , Wilson, D. R. and Seath, D. D, "An Experimental Investigation of the Parallel Vortex-Airfoil Interaction at Transonic Speeds," Paper submitted for presentation at AIAA 20th Fluid Dynamics, Plasmadynamics and Lasers Conference, Buffalo, NY, June 12-14, 1989.

4.0 SCIENTIFIC PERSONNEL

Dr. Donald R. Wilson, Principal Investigator

Dr. Donald D. Seath, Principal Investigator

Mr. I. M. Kalkhoran, Graduate Research Associate, Ph.D., December 1977

Mr. Y. Jung, Graduate Research Associate, Ph.D., August 1988.

Mr. H. S. Wang, Graduate Research Assistant, M.S., August 1986

Mr. J. M. Kim, Graduate Research Assistant, M.S., May 1986

Mr. A. Bharghava, Graduate Research Assistant, M.S., August, 1987

Mr. John Englehardt, Lab Assistant, B.S., May 1988

Mr. David Bryant, Lab Assistant, Undergraduate Student

Mr. J. H. Holland, Lab Technician

REFERENCES

1. Wilson, D. R., "Development of The University of Texas at Arlington Aerodynamics Research Center," AIAA Paper 88-2002, AIAA 15th Aerodynamics Testing Conference, San Diego, California, May 18-20, 1988.

2. Seath, D. D. and Wilson, D. R., "Vortex-Airfoil Interaction Tests," AIAA Paper 86-0354, AIAA 24th Aerospace Sciences Meeting, Reno, Nevada, January 6-9, 1986.

3. Jung, Y. and Seath, D. D., "Spanwise Displacement of a Line Vortex Above a Wing - A Simple Calculation Scheme," AIAA Journal of Aircraft, Vol. 25, No. 5, May 1988, pp. 476-478.

4. Seath, D. D., Kim, J. M. and Wilson, D. R., "An Investigation of Parallel Blade-Vortex Interaction in a Low- Speed Wind Tunnel," AIAA Paper 87-1345, AIAA

19th Fluid Dynamics, Plasma Dynamics and Lasers Conference, Honolulu, Hawaii, June 8-10, 1987.

5. Seath, D. D., Kim, J. M. and Wilson,D. R., "An Investigation of Parallel Blade-Vortex Interaction in a Low- Speed Wind Tunnel," Accepted for publication, AIAA Journal of Aircraft.

6. Wilson, D. R. and Chou, S. Y., "Development of the UTA High Reynolds Number Transonic Wind Tunnel," AIAA Paper 85-0315, AIAA 23rd Aerospace Sciences Meeting, Reno, Nevada, January 14-17, 1985.

7. Kalkhoran, I. M., "An Experimental Investigation of the Perpendicular Vortex-Airfoil Interaction at Transonic Speeds," Ph.D. Dissertation, The University of Texas at Arlington, December 1987.

8. Kalkhoran, I. M. and Wilson, D. R. and Seath, D. D., "An Experimental Investigation of the Parallel Vortex-Airfoil Interaction at Transonic Speeds," Paper submitted for presentation at AIAA 20th Fluid Dynamics, Plasmadynamics and Lasers Conference, Buffalo,, NY, June 12-14, 1989.

9. Cardonna, F. X., Laub, G. H. and Tung, C., "An Experimental Investigation of the Parallel Blade-Vortex Interaction," Paper presented at ARO Workshop on Blade-Vortex Interaction, NASA Ames Research Center, California, October 27-31, 1984.

10. Srinivasan, G.R., McCroskey, W. J. and Kutler, P., "Numerical Simulation of the Interaction of a Vortex with Stationary Airfoil in Transonic Flow," AIAA-84-0254, AIAA 22th Aerospace Sciences Meeting, Reno, Nevada, January 9-12, 1984.

11. Jones, H.E ., "The Aerodynamic Interaction Between an Airfoil and a Vortex in Transonic Flow," Paper presented at ARO Workshop on Blade-Vortex Interaction, NASA Ames Research Center, California, October 27-31, 1984.

APPENDIX A

CONFERENCE AND JOURNAL PUBLICATIONS

RESULTING FROM ARO GRANT DAAG29-84-K-0131

AIAA-86-0354

Vortex-Airfoil Interaction Tests

D. D. Seath and D. R. Wilson, The Univ. of Texas at Arlington, Arlington, TX

AIAA 24th Aerospace Sciences Meeting

January 6-9, 1986/Reno, Nevada

VORTEX-AIRFOIL INTERACTION TESTS

Donald D. Seath and Donald R. Wilson
Aerospace Engineering Department
The University of Texas at Arlington
Arlington, Texas 76019

Abstract

Low-speed wind tunnel tests were conducted of a pressure-tapped wing model that spanned the test section and was located downstream of a half-wing model that generated a tip vortex. Tests of this perpen-dicular vortex-airfoil interaction showed that the vortex caused a substantial change in the pressure distribution of the downstream wing and also exhib-ited a spanwise drift as it passed over the wing. The spanwise drift was in the same direction as the spanwise component of the induced flow at the wing surface, and may be attributed to an image effect, similar to the drifting apart of a wing's trailing vortices as they approach the ground.

Introduction

Interactions between airfoils and vortices are of particular interest to helicopter designers when predicting rotor performance. Flow visualization studies of rotor blades have reveled vortices from previous blades passing close to and sometimes intersecting a following blade. The interaction geometries appear to include all possible orientations between the blade and the axis of the vortex.

Perhaps the easiest interaction geometry to simulate in a wind tunnel is the so-called perpendicular interaction wherein the core of the vortex filament is perpendicular to the spanwise direction of the wing. This paper reports on the results of perpendicular vortex-airfoil interaction tests in a low-speed wind tunnel.

Experimental Set-up

The vortex-airfoil interaction tests were conducted in the UTA Low-Speed Wind Tunnel. The wind tunnel is a closed-return type and is capable of speeds up to approximately 200 ft per sec in its 3-foot-wide by 2-foot-high test section. A 6-foot-span, 10-inch-chord wing model (NACA 64A015 section) with chordwise pressure orifices on upper and lower surfaces at mid-span was placed across the tunnel with both ends extending through holes in the side walls, effectively end-plating the wing and allowing the wing to be moved in the spanwise direction, positioning the pressure orifices laterally relative to the position of the trailing vortex (See Fig. 1).

The trailing vortex was generated by a half-wing model with a 19.25-inch span and an 11-inch chord (approximately an NACA 0015 section), attached to the tunnel side wall 33 inches upstream of the test wing model. The half-wing model can be moved vertically, thus allowing vertical positioning of the trailing vortex relative to the downstream test wing model. A sting balance was used to measure the lift on the half-wing model.

A small Pitot tube probe was used to survey the wake of the half-wing model and determine the

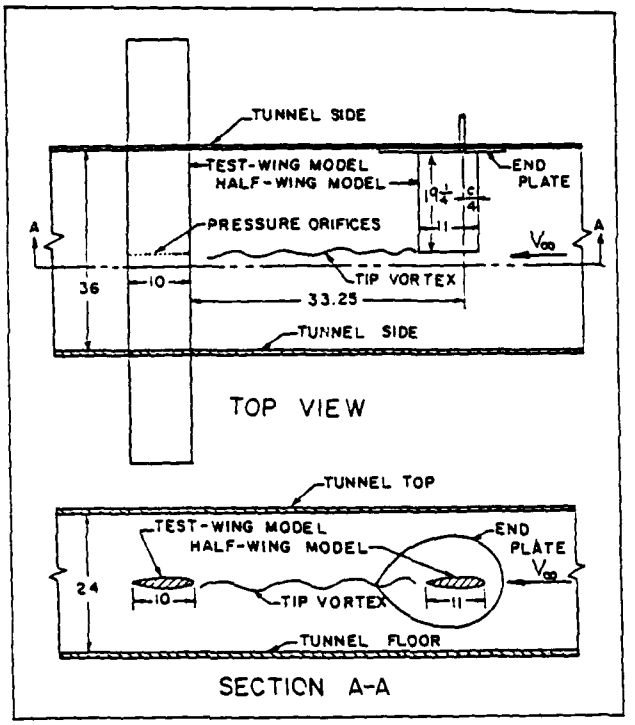

Fig. 1. Wind tunnel test set-up.
All dimensions in inches.

position of the trailing vortex by measuring the stagnation pressure deficit in the vortex core. Also, a flow field velocity survey of the trailing vortex was made with a 1/8-inch-diameter, five-hole, hemispherical-head pressure probe.

Oil-base artist paint was thinned with naptha and used to visualize the flow patterns on the upper surface of the downstream wing model as the trailing vortex passed nearby.

Tests Results

Low-speed wind tunnel tests were conducted with a free-stream dynamic pressure of approximately 11.1 psf and unit Reynolds number of 500,000 per ft. The downstream test wing was set at approximately zero angle of attack for all tests, and the vortex generator half wing was set at 5, 10, or 15 degrees angle of attack, with lift coefficients of 0.29, 0.65, and 0.99, respectively.

A reference pressure distribution for the airfoil at approximately zero angle of attack was taken without the vortex generator half-wing in tunnel and is presented in Fig. 2.

When the vortex generator wing was placed upstream of the airfoil the location of the trailing vortex was determined by means of a

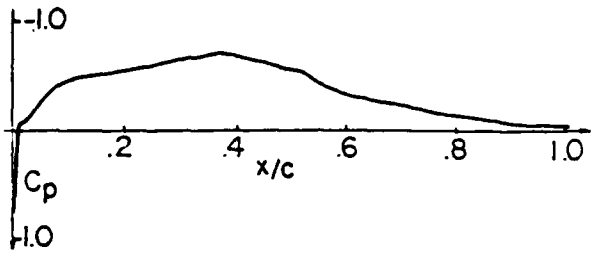

Fig. 2. Reference pressure distribution for airfoil w/o vortex

Pitot-tube survey. The point of minimum stagnation pressure on the Pitot tube was taken as the location of the center of the vortex core.

The position of the vortex core as it passed over the airfoil was measured at several chordwise stations and a typical path is shown in Fig. 3.

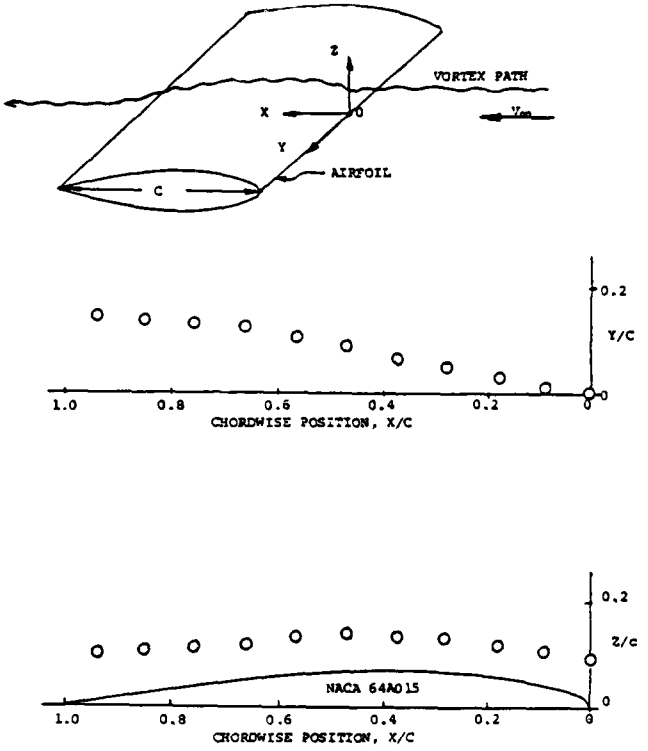

Fig. 3. Vortex position with respect to leading edge of airfoil. Vortex generator wing at 0.65 lift coefficient

The vortex lateral (spanwise) displacement from leading edge to trailing edge is called spanwise drift. The amount of spanwise drift depends on the strength of the vortex (which is a function of the lift on the vortex generator) and the vortex distance (height) above the airfoil. Measurements of vortex drift were made for three vortex strengths and various vortex heights and are presented in Fig. 4.

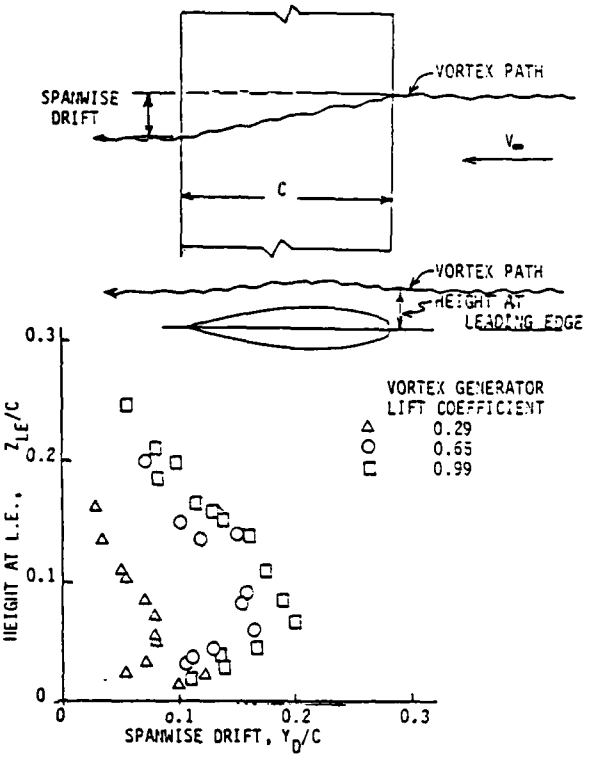

Fig. 4. Vortex spanwise drift

Visual verification of the vortex spanwise drift was accomplished by oil paint applied to the upper surface of the airfoil by means of a long tube with a rubber bulb on one end. The tube was loaded with the thinned-out paint and used to apply drops of paint on the airfoil surface while the tunnel was operating. Thus with a little practice, one could apply the paint at the proper locations, relative to the vortex, to visualize the flow separation and attachment lines on the airfoil. Figure 5 is a photograph of a surface oil flow pattern for a vortex generator at 10-degrees angle of attack and the vortex approximately 0.1 c above the airfoil as measured at the leading edge.

For reference purposes a white string was stretched over the airfoil after the flow pattern was established and the tunnel turned off. The string is directly under the measured vortex position at the leading edge and extends back to the trailing edge in a chordwise (streamwise) direction. Figure 6 shows a sketched interpretation of the oil flow pattern. The converging oil streaks indicate a separation line and the diverging streaks indicate an attachment line. The spanwise displacement of the separation and attachment lines indicates a spanwise drift of the vortex core above the airfoil surface. This spanwise drift is explained by the fact that a free vortex will move with the local flow field and therefore its axis will be aligned along a streamline. Because the trailing vortex passes close to the airfoil surface, there must (in effect) be an image vortex below the surface to cancel the perpendicular component of the flow induced by the vortex at the surface. This image vortex induces a lateral flow component at the trailing vortex position, causing the local flow to

Fig. 5. Photograph of surface oil flow pattern on airfoil with vortex passing above surface

have a spanwise component and deflecting the vortex in a spanwise direction (see sketch in Fig. 7). This situation is not unlike the spanwise movement of a trailing vortex as it approaches the ground.

An attempt is presently underway to predict the trailing vortex path by superimposing the image-induced velocity with the local velocity over an airfoil. The transverse velocity component of the trailing vortex, measured with a 5-hole pressure probe (without the airfoil present), is shown in Fig. 8. These results are considered preliminary at this time.

Since the position of the vortex over the airfoil is now known, the upper and lower surface pressures were measured directly under the vortex at several chordwise locations. These results are presented in Fig. 9 and show a definite effect of the vortex on the airfoil pressure distribution.

Conclusions

The results of these low-speed wind tunnel tests of an upstream-generated tip vortex trailing downstream past an airfoil, indicate two distinctive vortex-airfoil interaction effects. (1) The presence of the vortex induces a flow which decidedly changes the pressure distribution of the airfoil; (2) Also, the presence of the airfoil causes a lateral deflection (drift) of the vortex as it passes near the airfoil surface.

Future Work

Some of the results presented are from preliminary tests of the perpendicular vortex-airfoil interaction. Further detailed tests have been conducted and, whereas some of the quantitative

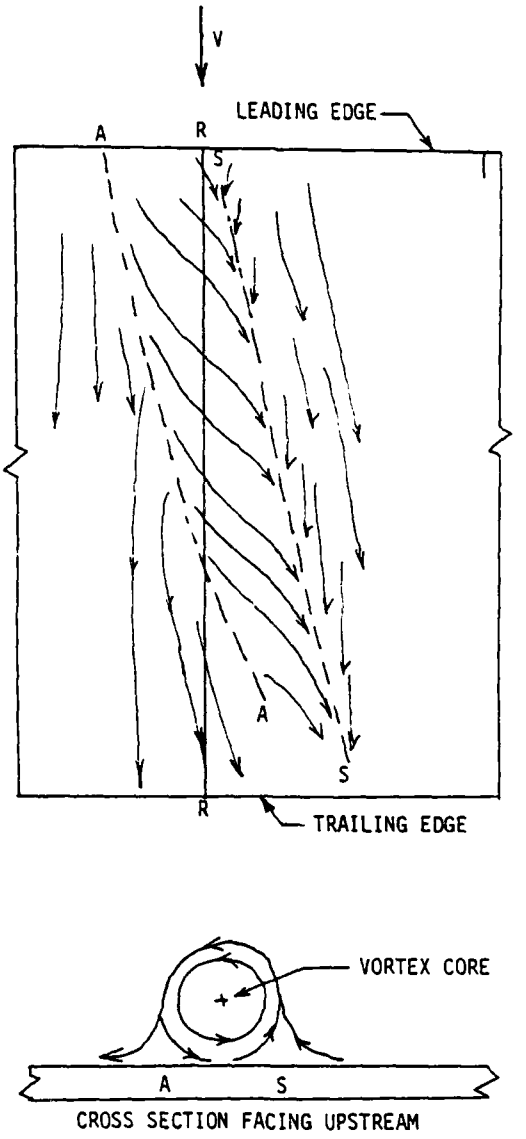

Fig. 6. An interpretation of the oil flow pattern in Fig. 5

results may change slightly, the qualitative results (trends) are not expected to change.

Tests are also being conducted in the UTA Transonic Wind Tunnel Facility to determine blade-vortex interactions in Mach number and Reynolds number ranges more representative of helicopter operations. Also, tests of parallel vortex-airfoil interactions are underway in the low-speed wind tunnel and are being planned for the transonic facility.

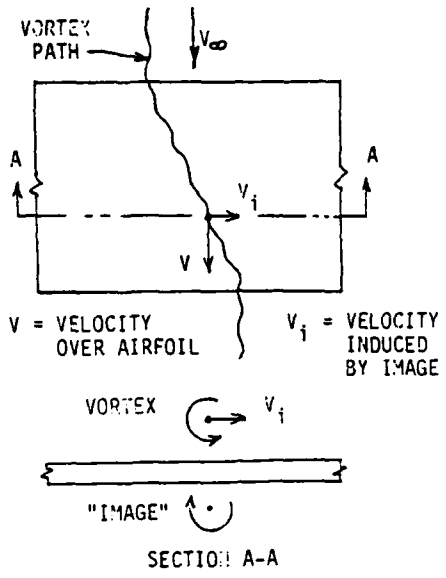

Fig. 7. Sketch of proposed flow field for vortex passing over wing

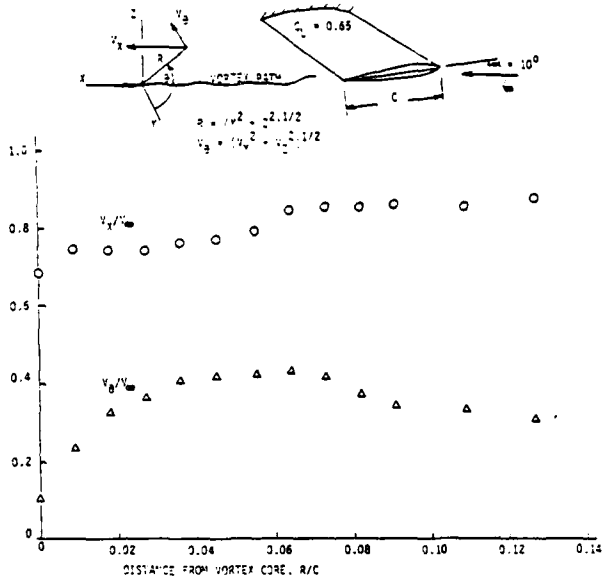

Fig. 8. Measured transverse velocity component in vortex

An in-house program to develop flow visualization capability via laser holographic interferometry is currently in progress, and will be implemented in forth coming investigation of the perpendicular blade-vortex interaction in the transonic Ludwieg tube tunnel. The technique bieng developed is similar to that used by Kittleson (Ref. 1) for obtaining holographic interferograms of the transonic field about a hovering rotor. A pulsed, frequency-doubled Nd:YAG laser will provide the optical source. Optical access is provided through

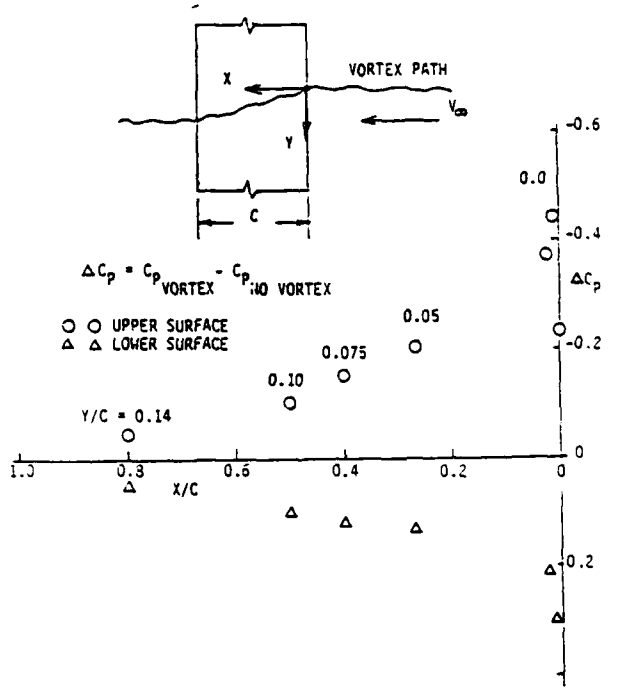

Fig. 9. Difference in pressure coefficient with and without vortex, measured directly under position (X,Y) of vortex above upper surface of airfoil. Vortex generator lift coefficient is 0.65 and vortex was approximately 0.09 C above airfoil at the leading edge.

3-inch diameter optical windows located at the airfoil mounting station. Both qualitative flow field visualization and quantitative density distributions are possible with this technique.

Acknowledgements

This work was supported by a grant from the Army Research Office, Contract DAAG29-84-K-0131, Experimental Simulation of Transonic Vortex-Airfoil Interactions. Scientific Liason officer is Henry Jones at the Army Aeroflight Dynamics Lab at Moffet Field, California.

Reference

1. K. K. Kittleson, "A Holographic Interferometry Technqiue for Measuring Transonic Flow Near a Rotor Blade," North European Rotorcraft Forum, Paper No. B, Stresa, Italy, September 13-15, 1983.

AIAA'87

AIAA-87-0208

An Experimental Investigation of the Perpendicular Vortex-Airfoil Interaction at Transonic Speeds

D. R. Wilson, I. M. Kalkhoran and
D. D. Seath, Univ. of Texas, Arlington, TX

AIAA 25th Aerospace Sciences Meeting

January 12-15, 1987/Reno, Nevada

AN EXPERIMENTAL INVESTIGATION OF THE PERPENDICULAR VORTEX-AIRFOIL INTERACTION AT TRANSONIC SPEEDS*

Donald R. Wilson+, Iraj M. Kalkhoran++, and Donald D. Seath+
The University of Texas at Arlington

ABSTRACT

Transonic vortex-airfoil interaction tests at Mach numbers ranging from 0.68-0.86 and airfoil Reynolds numbers of 3.8-5.5 million were conducted in the UTA high-Reynolds number, transonic Ludwieg tube wind tunnel. The scheme involves positioning a lifting wing (vortex generator) upstream of a NACA 0012 airfoil so that the trailing vortex interacts with the downstream airfoil. Tests were performed at several vortex strengths as well as several vortex core heights above the downstream airfoil. The results obtained from these experiments indicate a substantial change in the pressure distribution of the airfoil,a spanwise drift of the vortex core as it passes over the trailing airfoil similar to the results observed previously in low-speed wind-tunnel tests conducted at UTA, and a high degree of unsteadiness in the vicinity of the vortex core.

NOMENCLATURE

C	airfoil chord
C_p	pressure coefficient
$\bar{C}_p$	average pressure coefficient
C^*_p	critical pressure coefficient
d	vortex core diameter
h	vortex height above the airfoil
l	characteristic length
M	Mach number
P_t	total pressure
Re	Reynolds number
S	spanwise drift
T	Thompson number
t	time
V_∞	free stream velocity
x,y,z	cartesian coordinates
α_{VG}	vortex generator angle of attack
Γ	circulation

INTRODUCTION

A thorough physical understanding of the blade-vortex interaction (BVI) phenomena is necessary for the development of high-performance helicopter rotors. Not only does the trailing vortex system shed from one blade of a helicopter rotor exert a significant influence on the aerodynamic characteristics of the following blades (Refs. 1,2), but in addition, the blade-vortex interaction has been identified as the primary mechanism involved in the acoustic phenomenon known as "blade slap" (Refs 3-5).

A simple dimensional analysis of the blade-vortex interaction problem indicates that the governing simulation parameters are the rotor Mach number, Reynolds number and angle of attack; a vortex interaction parameter defined by $\Gamma/V_\infty C$, where Γ is the vortex circulation, V_∞ the rotor relative velocity and C the rotor chord; Thompson number, $T=t\ V_\infty/l$, where t is the flow relaxation time and l an appropriate characteristic length; and the pertinent geometric parameters describing the position of the vortex core and its interaction angle with the trailing rotor blade.

The specific objectives of this program were to develop experimental procedures and techniques for simulation of the perpendicular helicopter rotor blade-vortex interaction (BVI) phenomena in a Ludwieg tube wind tunnel at Mach numbers and Reynolds numbers representative of operational advancing rotor blade flight conditions, and to quantify the effects of vortex strength and height on both the structure of the vortex as it passes over the rotor and the aerodynamic characteristics of the rotor blade. Similar results from low-speed wind tunnel tests were reported in Ref. 6.

EXPERIMENTAL SETUP

The UTA high Reynolds number transonic wind tunnel (Figs. 1,2) is a Ludwieg tube tunnel designed to provide high Reynolds number transonic flows (Ref. 7). Maximum steady-state stagnation pressures of about 3.8×10^6 N/m^2 (550 psia) can be generated giving unit Reynolds numbers of up to 4×10^8 per meter (10 million per inch). The tunnel has a 18.5 x 23.2 cm (7.34 x 9.16 in.) rectangular, porous wall test section. The porosity is provided on all four walls and is set to a predetermined value prior to the run.

An instrumented NACA 0012 airfoil, spanning the entire height of the test section, is mounted vertically at the test section CMR, 43.18 cm (17 in.) downstream of the test section entrance. The airfoil has a 5.08 cm (2 in.) chord and is set 1.9 cm. (0.75 in) off centerline, with the lower surface closer to the test section wall. The model has approximately a 3.2 percent blockage in the test section. The airfoil is equipped with 13 absolute pressure transducers on the upper surface of the airfoil located at the midspan position (Fig. 3).

Facility operation and control, data acquisition, and data processing are accomplished by custom-designed micro-computers. A schematic of the system is shown in Fig. 4. The data acquisition/control computer (DAC) controls the operation of the tunnel and collects data from a 24-channel Kulite® high-frequency pressure transducer system, and stores the data within the computer memory. The stored data is transferred to the master computer for permanent storage on disks and subsequent data reduction.

* Work supported by ARO Grant DAAG29-84-K-131, Dr. Robert Singleton, contract monitor.
+ Professor, Aerospace Engineering, Associate Fellow, AIAA.
++ Graduate Research Associate, Aerospace Engineering, Student Member AIAA.

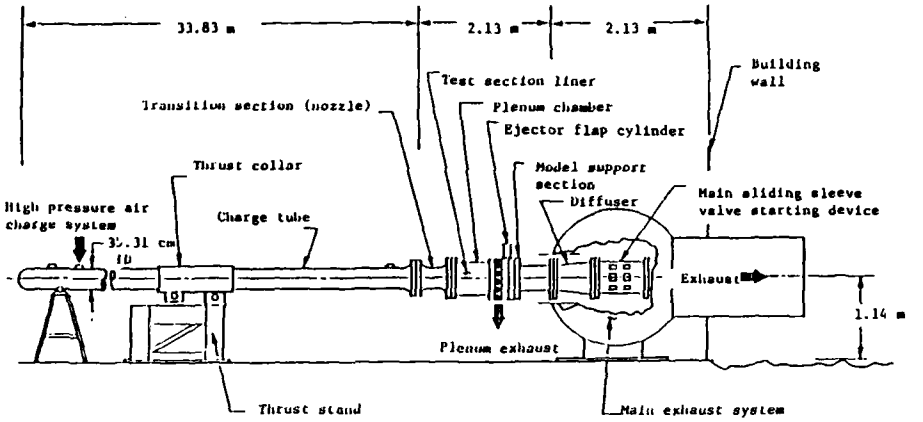

Fig. 1. UTA transonic Ludwieg tube tunnel-elevation line drawing

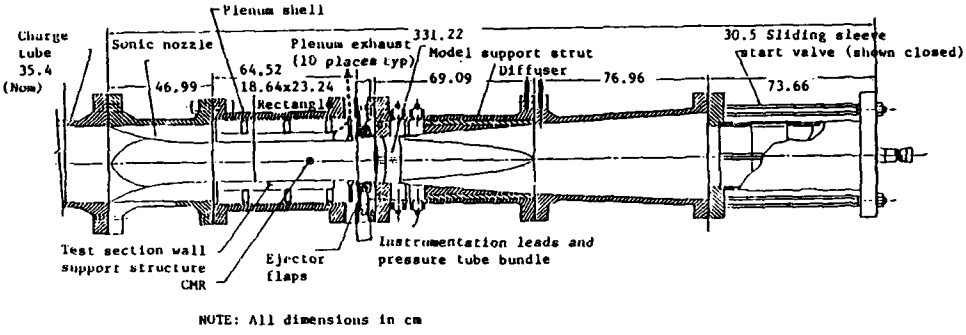

Fig. 2. Cross sectional view of nozzle, test section, diffuser, and main valve system

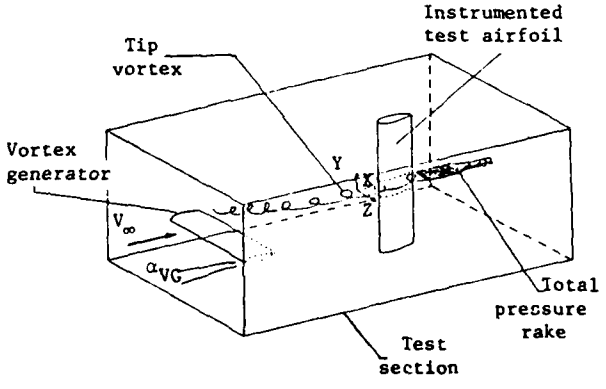

Fig. 3. Simulation of perpendicular vortex-airfoil interaction

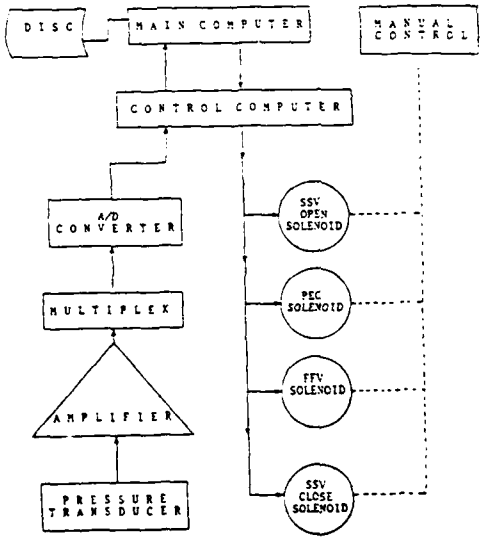

Fig. 4. Facility control/data acquisition system block diagram

The vortex was generated by a horizontally-mounted semi-span wing having a 5.08 cm (2 in.) chord, located at the entrance to the test section, which is approximately 9 chord lengths upstream of the test airfoil. The distance from the tip vortex core to airfoil surface was varied by using 3 different vortex generators with semi-spans of 12.95, 13.46, and 13.97 cm (5.1, 5.3 and 5.5 in.), corresponding to vortex heights of 30, 20 and 10 percent chord above the airfoil respectively. The vortex strength was varied by positioning the vortex generator at different angles of attack.

The location and detailed structure of the tip vortex were determined by use of a total pressure rake and a five-hole cone probe. The total pressure rake contained 13 total pressure probes with 0.32 cm (0.125 in.) spacing. The five-hole cone probe was equipped with a total pressure orifice at the nose and four equally spaced ports on the cone surface. This probe was used primarily to verify the data obtained from the total pressure rake and to obtain information concerning the vortex viscous core size and symmetry.

TUNNEL CALIBRATION

The test section static pressure distribution and its relationship to the surrounding plenum chamber pressure was determined prior to the interaction runs. The test section static pressure was measured by means of a standard centerline pipe and the stagnation pressure measurements were performed in the charge tube using total pressure probes (Ref. 7). The test section Mach number was varied primarily by changing the ratio of the secondary exhaust flow to the flow through the test section. This is accomplished by changing the area of the exhaust flow via a variable orifice ball valve.

The calibration tests were conducted at Mach numbers ranging from 0.68 to 0.86 for a range of charge tube pressures. The results of the calibration tests are illustrated in Fig. 5. Figure 5a shows the test section uniformity for different ball valve positions; while Fig. 5b is the summary of the calibration data indicating the test section and plenum chamber Mach number relationship. The

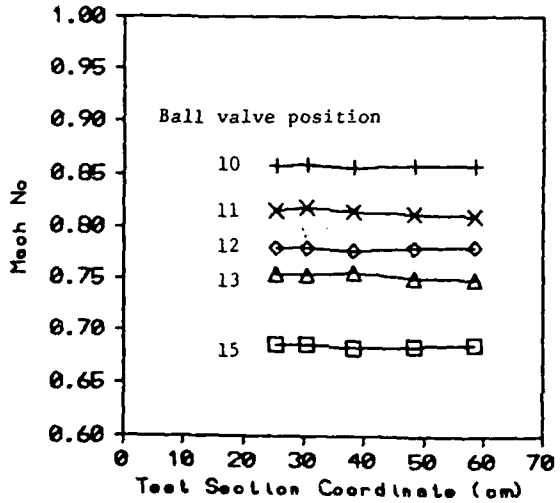

a. Axial Mach number variation

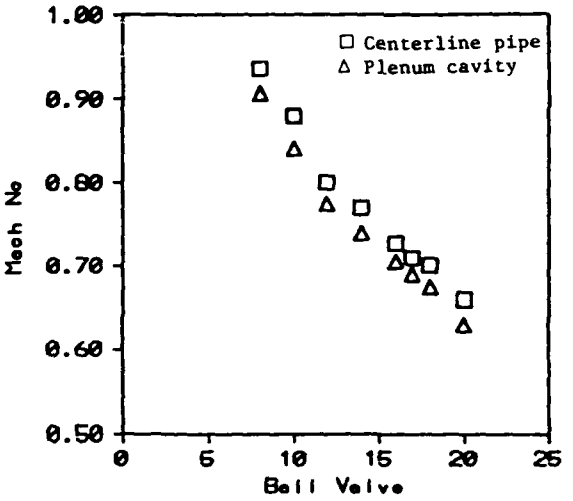

b. Test section Mach number variation with ball valve position

Fig. 5. Transonic wind tunnel test section calibration

relationship between the test section and plenum Mach number was used to estimate the free stream Mach number in all of the subsequent experiments.

AIRFOIL CALIBRATION

The airfoil calibration tests for a range of Mach and Reynolds numbers were conducted prior to the vortex-airfoil interaction tests. The major objective of this program was to verify the accuracy and the repeatability of the test data. Figure 6 illustrates the comparison between the results of the current study and the data of Ref. 8. Considering the small discrepancy in the angles

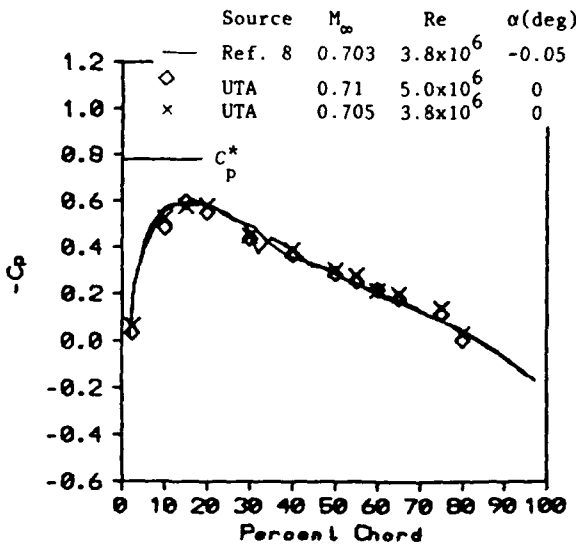

Fig. 6. Comparison of measured upper surface pressure distributions with data of Ref. 8

of attack, the agreement is quiet good. Repeatability of the airfoil pressure distribution data for the Ludwieg tube tunnel is illustrated in Fig. 7, where the upper surface pressure distributions from three different runs at essentially identical test conditions are compared.

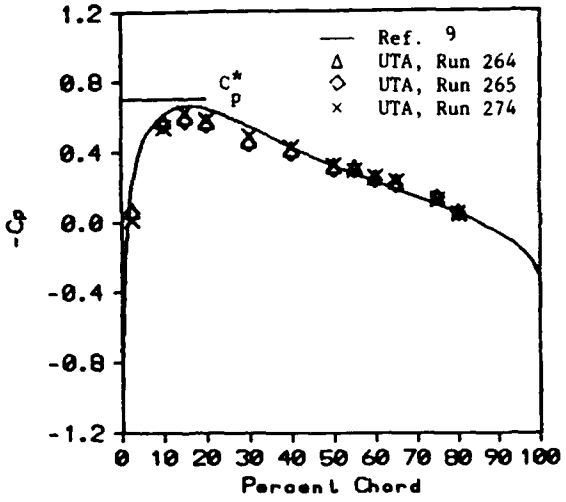

Fig. 7. Repeatability of pressure distribution data: M=0.72, Re=5x10^6

VORTEX SURVEY

To determine the vortex core geometric position, i.e the location of the vortex core above the airfoil (Z_v) and along the span (Y_v), the total pressure rake was placed downstream of the vortex generator, with the total pressure probes spanning a segment of the flow in the Z direction. Two-dimensional mapping of the vortex was then accomplished by positioning the rake at different spanwise positions for subsequent wind tunnel firings. Typical results from the total pressure rake survey of the vortex structure are shown in Fig. 8. Figure 8a shows a horizontal pressure

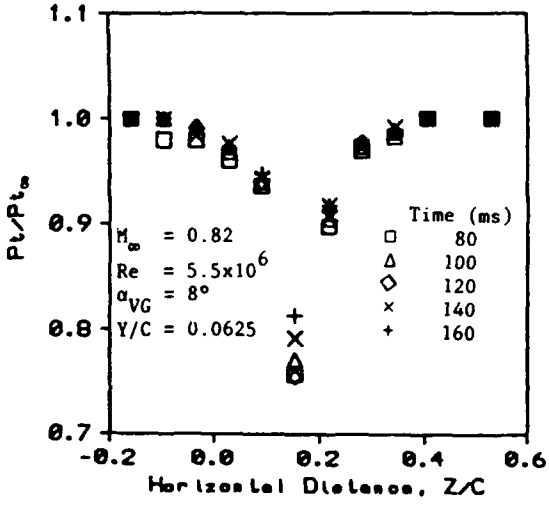

a. Horizontal total pressure survey through vortex core

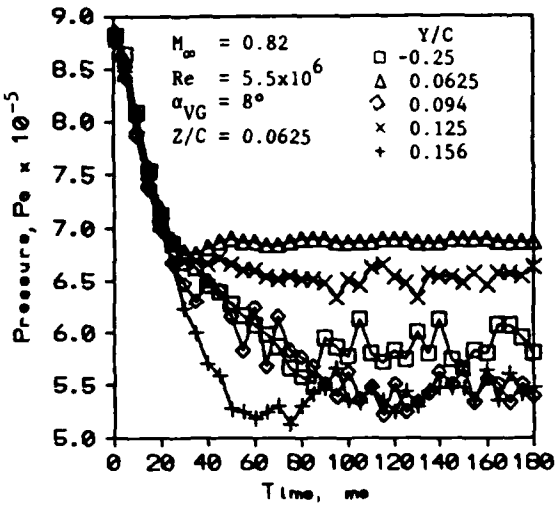

b. Total pressure vs time at selected vertical locations

Fig. 8. Vortex survey: M=0.82, Re=5.5x10^6, α_{VG}=8°

survey through the core of the vortex. Two points are immediately obvious. First, the vortex appears to have a well-defined core, with the total pressure deficits in the core region on the order of 20 to 25 percent of the test section total pressure. Second, the results of the rake survey indicate a substantial amount of unsteadiness near the vortex core. Selected pressure vs time traces are shown in Fig. 8b for various probe locations. These traces (obtained by scanning the pressure transducer output at 1 msec time intervals) show considerable pressure fluctuations near the center of the vortex, however these fluctuations tend to damp out at distances further away from the vortex center. The fluctuations in pressure are thought to be a result of oscillation of the vortex core about a mean position. Time-mean averaging of the pressure traces (after completion of the tunnel starting transient) gives a steady mean value, and these data have been used to generate the constant total pressure contour map of Fig. 9.

In order to determine the vortex symmetry and its viscous core size (d/C), five-hole cone probe surveys through the vortex core were conducted. Figure 10 is produced by differencing the pressures of the two opposing ports on the surface of the cone probe. A fairly symmetric vortex structure with a well defined core can be seen in this figure. The nondimensional viscous core diameter is approximately 0.25 (d/C=0.25).

VORTEX-AIRFOIL INTERACTION

The vortex-airfoil interaction measurements were primarily in the form of pressure distribution changes on the upper surface of the airfoil. The generated vortex always passed over the instrumented upper surface of the downstream airfoil. The effect of vortex strength on the pressure distribution of the airfoil is illustrated in Fig. 11a, where the results obtained from 3 different vortex generator angles of attack are compared to the vortex-free pressure distribution. A sub-

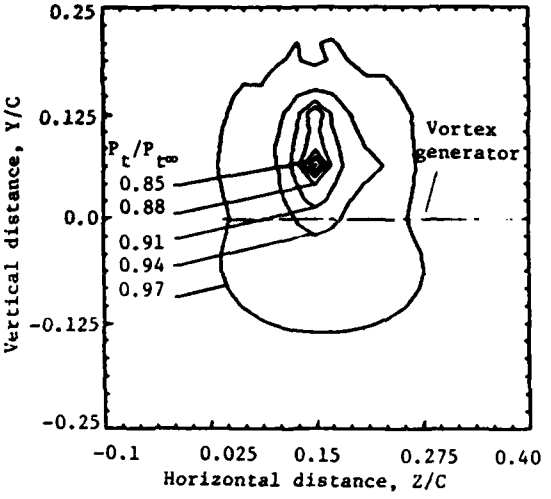

Fig. 9. Time-averaged total pressure contour map: M=0.78, Re=5.3x10^6, α_{VG}=8°

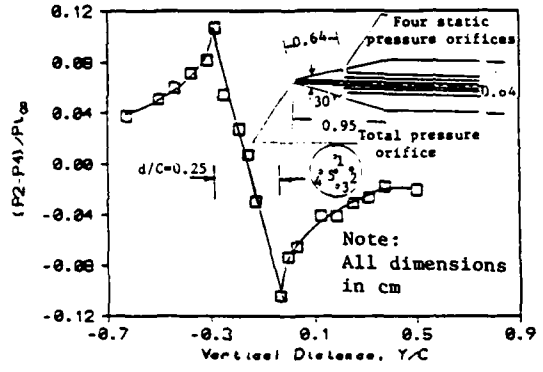

Fig. 10. 5-Hole cone probe survey of vortex core: M=0.74, Re=5.1x10^6, α_{VG}=8°

stantial change near the leading edge of the airfoil, where the pressure gradient in the Z direction is large, is quiet evident. This effect is caused by the pressure difference between the low pressure vortex core region and the higher pressure region near the airfoil leading edge. The effect of the vortex tends to damp out at downstream distances and the flow is dominated by the vortex-free mean flow. One explanation for this behavior is the spanwise drift of the vortex after interacting with the downstream airfoil, which will be discussed in the following section. Also of vital importance are the vortex-breakdown and flow separation phenomenon, which were experimentally observed by flow visualization for similar interaction problems by several investigators (Ref. 10). Figures 11b and 11c indicate the same trend for free stream Mach numbers of 0.72 and 0.78 respectively, which correspond to the critical and super-critical free stream Mach numbers. A more pronounced change in the pressure distribution of the downstream airfoil is observed when the airfoil is set to a 2-degree angle of attack. Locally vortex-induced supersonic and separated flow regions near the airfoil leading edge (2.5 % C) are shown in Fig. 11d.

To determine the effect of the vortex core height above the airfoil, tests were conducted using 3 vortex generator semi-spans which yield vortex heights of 10, 20 and 30 percent of the airfoil chord at the airfoil leading edge. Figure 12 shows the results of this study, where a progressive increase in the magnitude of the pressure coefficient near the leading edge is observed as the vortex height above the upper surface of the airfoil is reduced. Also evidence of local flow separation near the 70 percent chord position is observed for the closer encounters. The aforementioned results discussed for typical

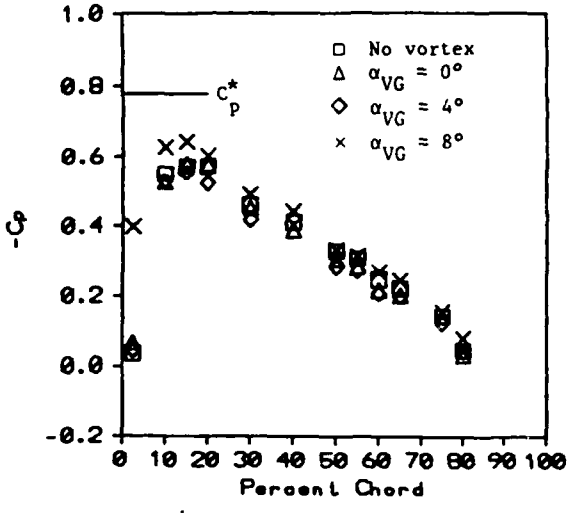

a. Airfoil angle of attack of 0°: M=0.70, Re=5.1x10^6, h/C=0.1

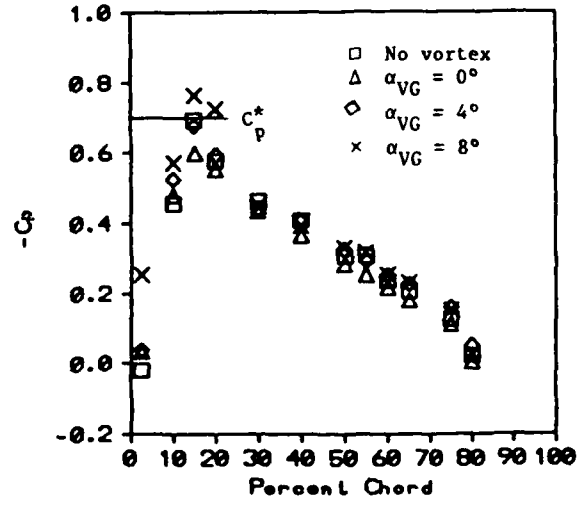

b. Airfoil angle of attack of 0°: M=0.72, Re=5.2x10^6, h/C=0.2

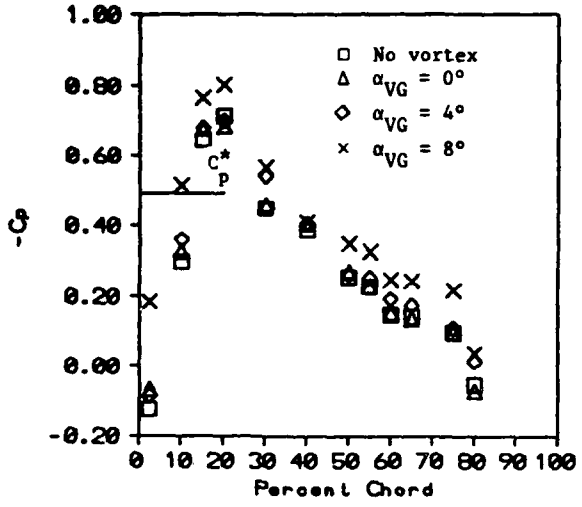

c. Airfoil angle of attack of 0°: M=0.78, Re=5.2x10^6, h/C=0.20

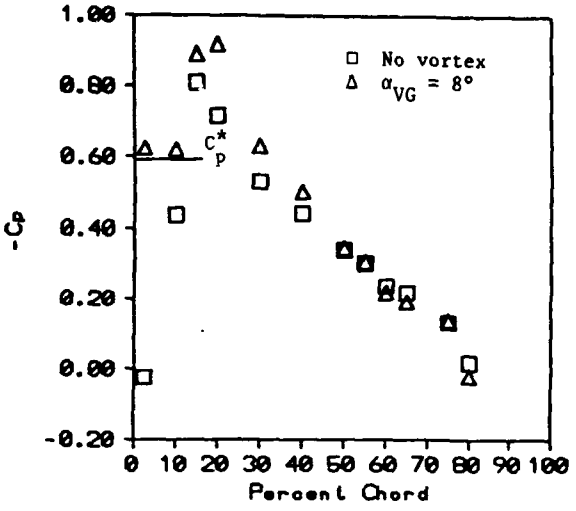

d. Airfoil angle of attack of 2°: M=0.75, Re=5.2x10^6, h/C=0.10

Fig. 11. Effect of vortex strength on airfoil pressure distrbution

vortex strengths and heights above the airfoil are qualitatively similar for all Mach and Reynolds numbers tested throughout this study.

The variation of Reynolds number, as shown in Fig. 13, does not appear to have a significant effect on the pressure distribution of the downstream airfoil, for the range of Reynolds numbers (3.8-5.4 million) tested during this program.

The combined effects of Mach number and vortex height on the aerodynamic characteristics of the downstream airfoil are shown in Fig. 14, where the C_p plots are integrated along the chord to yield an average upper surface pressure coefficient, $\bar{C}_p$. As the vortex height above the airfoil is reduced, a

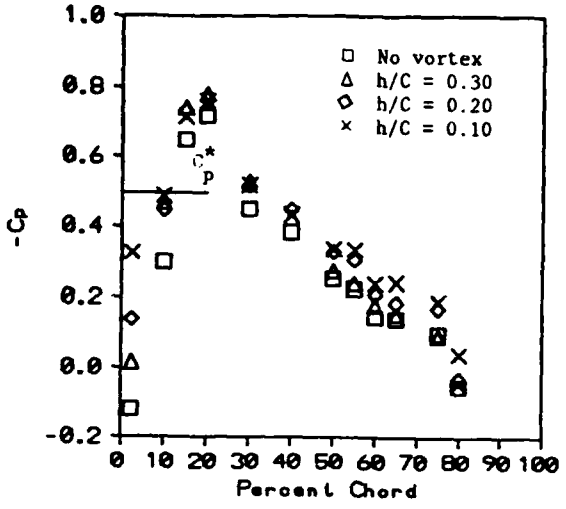

Fig. 12. Effect of vertical height of vortex core above airfoil surface: M=0.78, Re=3.9x10^6, α_{VG}=8°

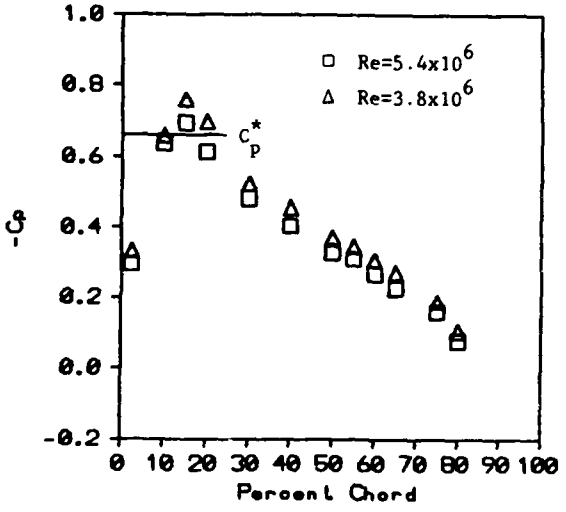

Fig. 13. Effect of Reynolds number variation: M=0.78, α_{VG}=8°, h/C=0.20

progressive decrease in the magnitude of the average pressure coefficient is evident. A $\bar{C}_p$ decrease in excess of 30 percent for the closest encounter at a free stream Mach number of 0.71 is shown in Fig. 14, while this decrease is only slightly over 20 percent for a Mach number of 0.77 for the same vortex core height.

STRUCTURE OF THE VORTEX

The structure of the vortex after interacting with the airfoil was examined by conducting rake pressure surveys at both the leading and the trailing edges of the downstream airfoil. The results are in qualitative agreement with the low-speed test results of Ref. 6, and a spanwise drift of the vortex core is observed as the vortex passes over the airfoil. An explanation for this behavior based on an image vortex model is presented in

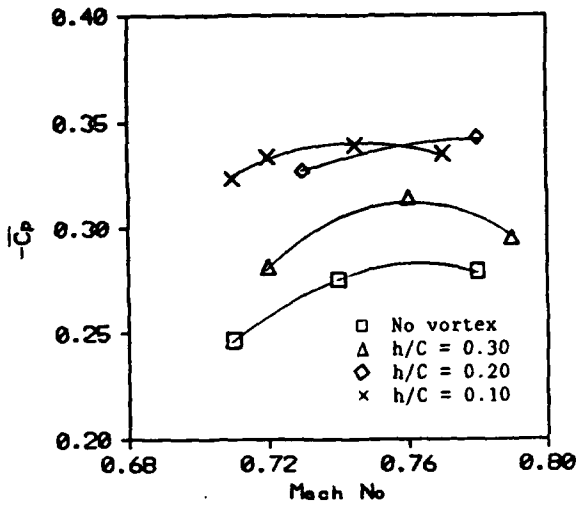

Fig. 14. Average pressure coefficient variation for several vortex core heights

Ref. 6. Figure 15 shows the results of the rake surveys at both the leading and trailing edges for a vortex core height (h/C) of 0.30. The spanwise drift of the minimum pressure location on the rake from leading edge to trailing edge is 0.46 cm (0.18 in.). This spanwise drift is found to be dependent on the vortex height above the airfoil.

Time-mean average total pressure contour maps of the vortex at the airfoil leading and trailing edges are shown in Fig. 16 for h/C=0.30. Similar contour maps for vortex heights of 20 and 10 percent at the airfoil trailing edge are shown in Figs. 17 and 18 respectively. For the case of the closest encounter (h/C=0.10) the interaction between the vortex core and the airfoil wake is quiet strong (Fig. 18), but due to the narrow size of the airfoil wake the vortex core is easily distinguished by its wider band.

An examination of the contour maps at the trailing edge of the airfoil indicates an increase in the spanwise deflection of the vortex core, as the height of the core above the airfoil is reduced. This effect is illustrated in Fig. 19, which presents the measured spanwise drift of the core of the vortex as a function of the vortex core height at the leading edge. Similar results were presented in Ref. 6 for low-speed tunnel simulation of the vortex-airfoil interaction; and in fact, the magnitude of the drift for comparable vortex core heights is quite comparable.

The contour maps also indicate the appearance of two distinct minimum total pressure regions separated by some distance at the intermediate core height. The presence of these low total pressure regions suggests the possibility of formation of a secondary vortex caused either by the breakup of the primary vortex into two vortices or by formation of secondary vortex caused by the separation of the flow due to vortex airfoil interaction (separation vortex). The secondary vortex observed for a vortex height of 0.20 (h/C=0.20), is not seen for the closest encounter (h/C=0.10). The exact reason for this is not known at this time. Due to the strong interaction of the vortex with the wake of the downstream airfoil, the secondary vortex might be absorbed within the low total pressure region in the wake of the downstream airfoil, and not detectable by total pressure measurements alone.

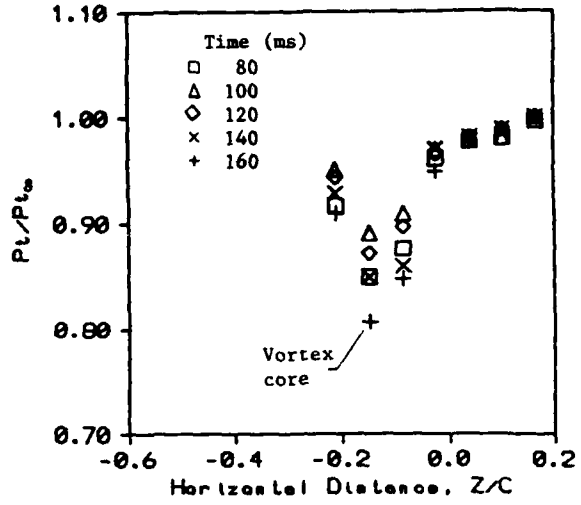

a. Total pressure survey at leading edge: M=0.72, Re=5.1x10^6, α_{VG}=8°, h/C=0.30

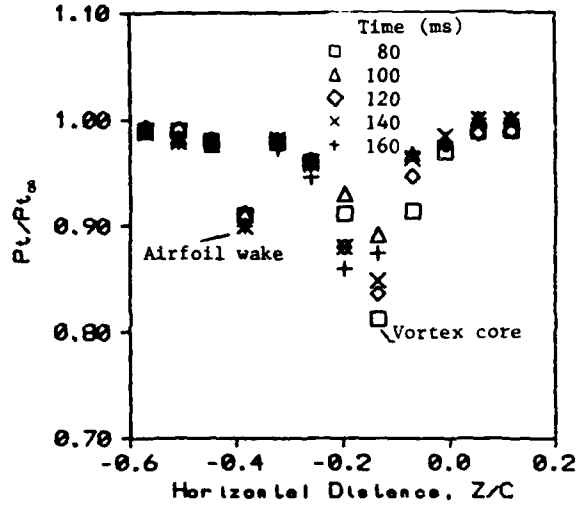

b. Total pressure survey at trailing edge: M=0.72, Re=5.1x10^6, α_{VG}=8°, h/C=0.30

Fig. 15. Vortex structure in the local vicinity of the airfoil

Further tests with the 5-hole cone probe are planned to provide detailed mapping of the vortex structure at the trailing edge of the airfoil.

CONCLUDING REMARKS

The experimental data obtained from the transonic vortex airfoil interaction tests indicates that (1) The trailing vortex in transonic flows contains a high degree of unsteadiness, particularly in the vortex core region; (2) Interaction of the vortex with the downstream airfoil substantially alters the pressure distribution of the downstream airfoil. This effect is found to be a function of vortex strength and geometric posi-

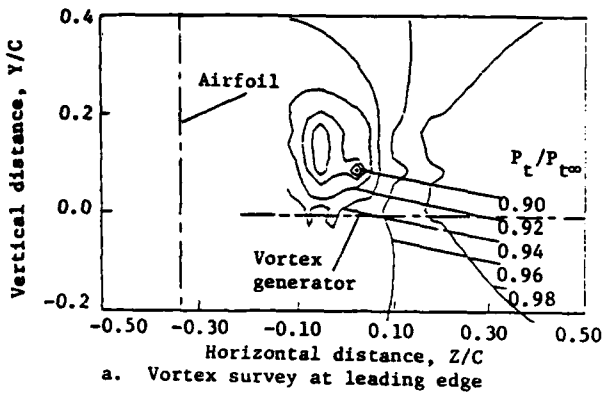

a. Vortex survey at leading edge

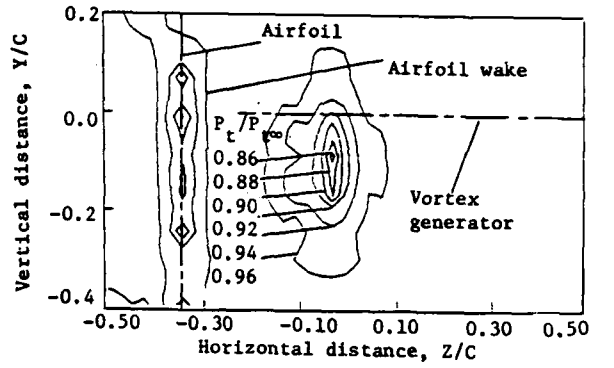

b. Vortex survey at trailing edge

Fig. 16. $P_t/P_{t\infty}$ contour map at leading and trailing edge for M=0.72, Re=5.1x10^6, α_{VG}=8°, h/C=0.30

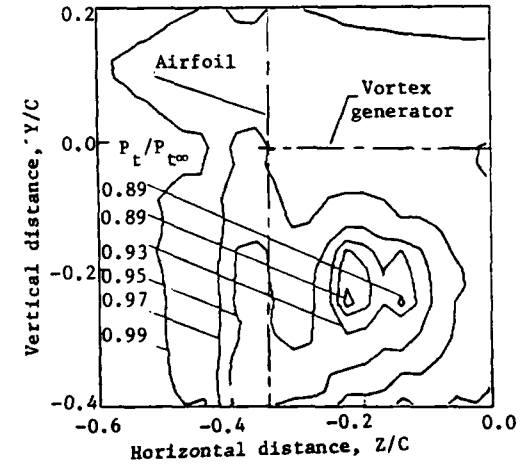

Fig. 17. $P_t/P_{t\infty}$ contour map at airfoil trailing edge for M=0.72, Re=5.1x10^6, α_{VG}=8°, h/C=0.20

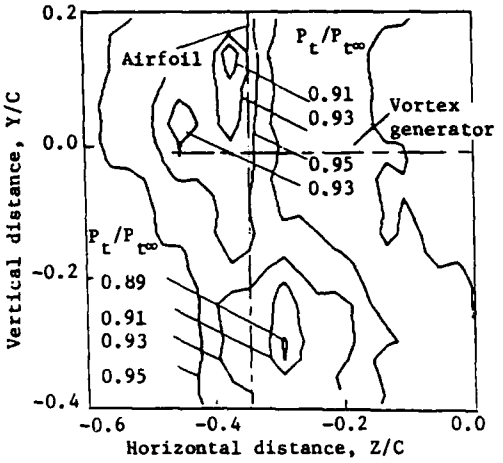

Fig. 18. $P_t/P_{t\infty}$ contour map at airfoil trailing edge for M=0.72, Re=5.1x10^6, α_{VG}=8°, h/C=0.10.

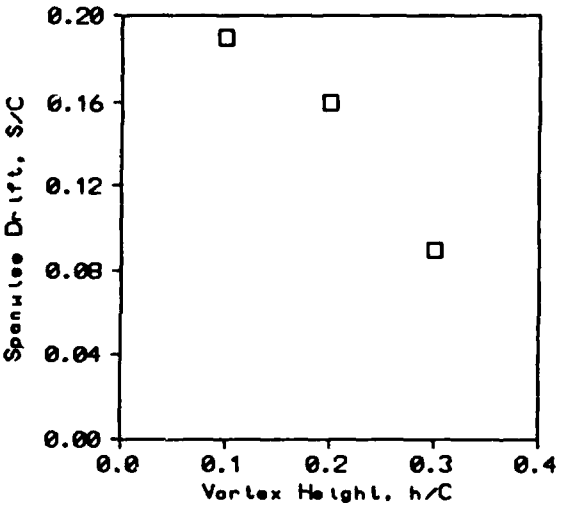

Fig. 19. Spanwise drift of the vortex center: M=0.75, Re=5.2x10^6, α_{VG}=8°

tion relative to the downstream airfoil, but relatively insensitive to the Reynolds number; (3) The downstream airfoil causes a spanwise drift in the vortex core and the amount of drift tends to increase for cases where the vortex is closer to the airfoil surface; and (4) Formation of a secondary vortex is observed as the vortex approaches closer to the airfoil surface.

REFERENCES

1. Landgrebe, A. J. and Cheney, M. C., Jr., "Rotor Wakes-Key to Performance Predictions," Aerodynamics of Rotary Wings, AGARD CP-111, Feb. 1973.

2. McCroskey, W. J., "Some Current Research on Unsteady Fluid Dynamics," Trans. ASME, Journal Fluid Engr., Vol. 99 Series 1, No 1, March 1977, pp. 8-38.

3. Widnall, S., "Helicopter Noise Due to Blade-Vortex Interaction," Jour. Acoustical Society of America, Vol. 50, No. 1, Pt. 2,1971.

4. Leighton, K. P., "Research on Model Helicopter Blade Slap at Moderate Tip Speeds," Jour. American Helicopter Society, Vol. 27, No. 3, July 1982, pp. 11-17.

5. Boxwell, D. A. and Schmitz, F. H., "Full-Scale Measurement of Blade-Vortex Interaction Noise," Jour. American Helicopter Society, Vol. 27 No. 4 Oct. 1982, pp. 11-27.

6. Seath, D. D. and Wilson, D. R. ," Vortex-Airfoil Interaction Tests," AIAA Paper 86-0354, AIAA 24th Aerospace Sciences Meeting, Reno NV, January 1986.

7. Wilson, D. R. and Chou, S. Y., "Development of the UTA High Reynolds Number Transonic Wind Tunnel," AIAA Paper 85-0315, AIAA 23rd Aerospace Sciences Meeting, Reno NV, January 1985.

8. Ohman., L. H., "Experimental Data Base for Computer Program Assessment," AGARD-AR-138, May 1979.

9. Lock, R. C., "Test Cases for Numerical Methods in Two-Dimensional Transonic Flows," AGARD Rept. 575, 1970.

10. Patel, M. H. and Hancock, G. J., "Some Experimental Results of the Effect of a Streamwise Vortex on a Two-Dimensional Wing," Aeronautical Journal, April 1974, pp 151-155.

J. K. L.

AIAA'87

AIAA-87-1345
An Investigation of the Parallel Blade-Vortex Interaction in a Low-Speed Wind Tunnel

D.D. Seath, Jai-Moo Kim and D.R. Wilson, Univ. of Texas, Arlington, TX

AIAA 19th Fluid Dynamics, Plasma Dynamics and Lasers Conference

June 8-10, 1987/Honolulu, Hawaii

AN INVESTIGATION OF THE PARALLEL BLADE-VORTEX INTERACTION IN A LOW-SPEED WIND TUNNEL

Donald D. Seath,* Jai-Moo Kim,** and Donald R. Wilson*
The University of Texas at Arlington
Arlington, Texas 76019

Abstract

Low-speed wind tunnel tests were conducted to investigate the parallel blade-vortex interaction. Flow visualization tests of vortex generation performed prior to the pressure tests showed that a well defined starting vortex was generated by an impulsively pitched wing.

Time history of the pressure distribution on a pressure-tapped wing model was acquired as the starting vortex passed over the wing. These pressure tests revealed that a substantial pressure change near the leading edge was induced by the encountering vortex. The effects of vortex proximity, reduced frequency and maximum pitch angle of the vortex generator on the pressure change were also investigated.

Nomenclature

α	Pitch angle of vortex generator
α_{max}	Maximum pitch angle of vortex generator
$\dot{\alpha}$	Pitch rate of vortex generator
c	Chord length of instrumented wing
$c_{v.g.}$	Chord length of vortex generator wing
C_ℓ	Section lift coefficient of instrumented wing
C_p	Pressure coefficient of instrumented wing, $(P-P_\infty)/q$
k	Reduced frequency, $\dot{\alpha}c_{v.g.}/V_\infty$
P	Local static pressure
P_{ini}	Initial local static pressure
P_{max}	Maximum local static pressure
P_{min}	Minimum local static pressure
P_∞	Free stream static pressure
q	Free stream dynamic pressure
Re	Reynolds number
T	Time elapsed after vortex generation
V_∞	Free stream velocity
x	Longitudinal distance from instrumented wing leading edge to pressure tap
x_v	Longitudinal distance from instrumented wing leading edge to vortex center
y_v	Vortex generator height (See Fig. 9)
Γ	Vortex strength

INTRODUCTION

Helicopter rotors, either while hovering or in forward flight, encounter complex rotor flows such as separation, reverse flow, radial flow, aeroelastic response, transonic shocks, rotor wake and tip vortex-blade interaction as shown in Fig. 1 [1].*** Of these complex rotor flow problems, blade-vortex interaction has been an important research subject in fundamental rotor aerodynamics since it was identified as a helicopter impulsive noise source in addition to the high advancing blade Mach number [2]. The blade-vortex interaction noise is apt to occur when the helicopter is in powered descending motion [3]. To date, the acoustic formulation of the blade-vortex interaction noise has been well developed, however, the complex aerodynamic data for the input to the acoustic formulation are not provided sufficiently. Also the computational work has improved a number of finite difference schemes to simulate the blade-vortex interaction. Most of these schemes have modeled two-dimensional flow [4].

The helicopter rotor blade produces a differential pressure field across the blade in order to support the weight and provide thrust for forward flight. It leaves behind a continuous vortex sheet because of the lift variation along the blade span. This vortex sheet usually rolls up into two concentrated vortices, the tip vortex and the hub vortex. The hub vortex is carried down by the inflow and is relatively far removed from the blade path. Therefore the blade-vortex interaction with the hub vortex will not occur generally and only the tip vortex interaction needs consideration [7].

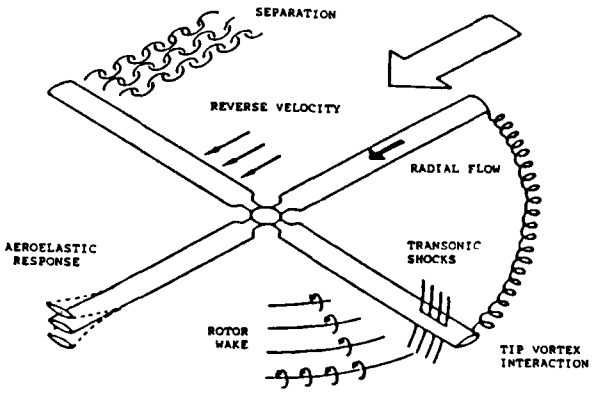

Fig.1 Complex Rotor Flows (Ref.1)

When a following blade intersects a tip vortex from a preceding blade, it causes an unsteady aerodynamic load on the rotor that is thought to radiate the blade-vortex interaction noise. The intersection angle between the vortex filament and the blade span of the following blade ranges from zero to 90 degrees. The zero-degree intersection produces the parallel blade-vortex interaction, as shown in Fig.2 from Ref. 4, and the 90-degree intersection produces the perpendicular interaction. The intersection angle appears to be related to the intensity of the acoustic pulse with the low-angle or parallel intersection producing a more intensive pulse. This phenomenon has been investigated experimentally and analytically for years [8,9].

---

*Professor of Aerospace Engineering
**Graduate Research Assistant, AE Department.
***Numbers in [ ] refer to references.

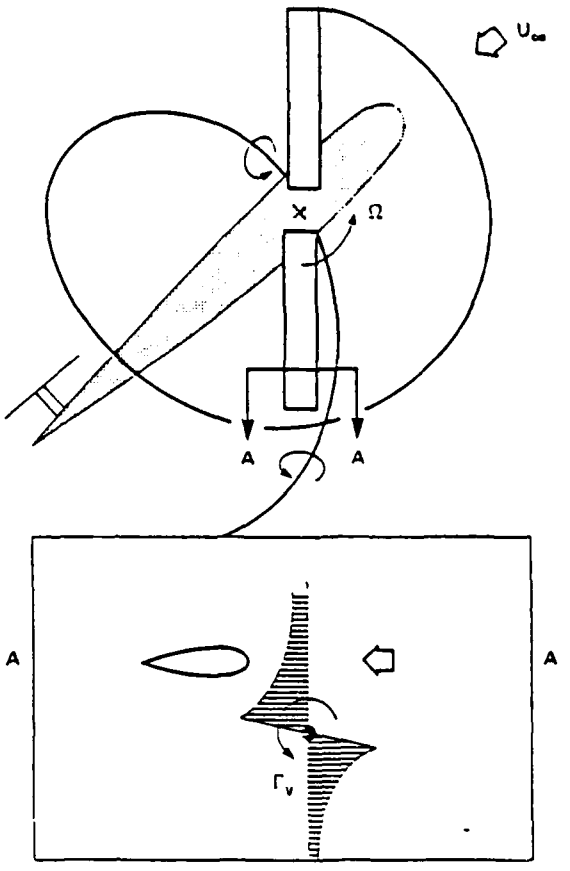

Fig.2 Parallel Blade Vortex Encounter [4]

Widnall developed a theoretical model for blade-vortex interaction in which the unsteady lift distribution computed on a two-dimensional airfoil passing obliquely over an infinite line vortex was taken as the boundary condition on a finite blade in the calculation of the acoustic farfield [9]. With this theoretical model, she showed that an increase in blade-vortex intersection angle decreased the unsteady signal and the decreased unsteady signal reduced the peak-to-peak pressure of the transient acoustic signal [10].

Considering that the parallel blade-vortex interaction is the main source of the helicopter impulsive noise and that most analytical and computational works for blade-vortex interaction have been performed in two-dimensional cases, it was decided that the experimental investigation should start with the limiting case of interest i.e. two-dimensional blade-vortex interaction.

Surendriah [5] used a half wing as a vortex generator and an instrumented rotating blade in a low-speed wind tunnel (Fig. 3) to investigate blade-vortex interaction.

The same scaled-up version of Surendriah's test method was performed at the U.S. Army Aeromechanics Laboratories' 7- by 10-foot Wind Tunnel at Ames Research Center [4].

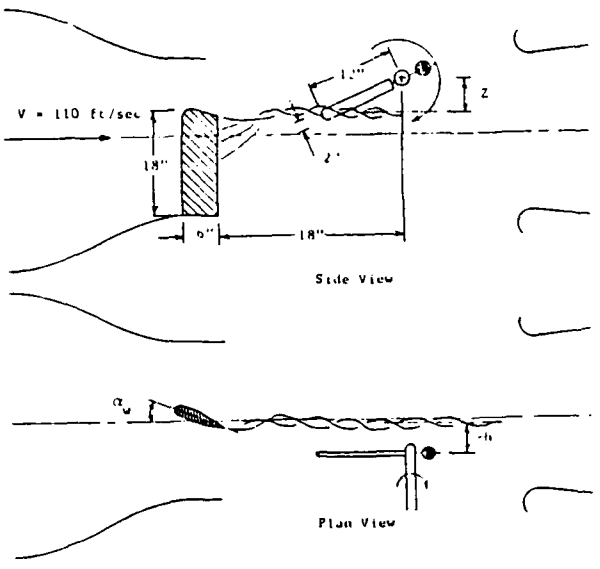

Fig. 3. Surendriah's Test Set-Up for Blade-Vortex Interaction Test [5]

In another wind tunnel simulation, Booth and Yu [11] utilized a sinusoidally oscillating wing for a vortex generator and placed a stationary wing downstream to simulate the advancing rotor blade. The flow visualization study of this test set-up revealed that a pair of vortices were generated from the vortex generator, and therefore was not equivalent to an isolated tip vortex encountering a rotor blade.

In the present tests, an impulsively-pitched wing in a low-speed wind tunnel was used to generate a starting vortex at its trailing edge. This vortex convected downstream, passed close to an airfoil (blade) and thus simulated the parallel blade-vortex interaction. For a more complete description of the tests, see Kim's thesis [12].

EXPERIMENTAL PROGRAM

The parallel blade-vortex interaction tests were conducted in the UTA Low-Speed Wind Tunnel. The vortex generator consisted of a 3.5-inch-chord, 18-inch-span (NACA 0012 section) half wing as shown in Fig. 4. End plates were attached to produce a more uniform spanwise lift distribution. The wing was mounted on a 1.5-inch-diameter aluminum shaft. In order to rapidly pitch the wing, a spring was connected between the wind tunnel wall and a moment-arm bolt on the shaft. Two stopper bolts were used to set the initial zero angle and the maximum pitch angle as shown in Fig. 5. The vortex-generator wing was constructed of composite materials to minimize the moment of inertia. The total vortex generator was attached

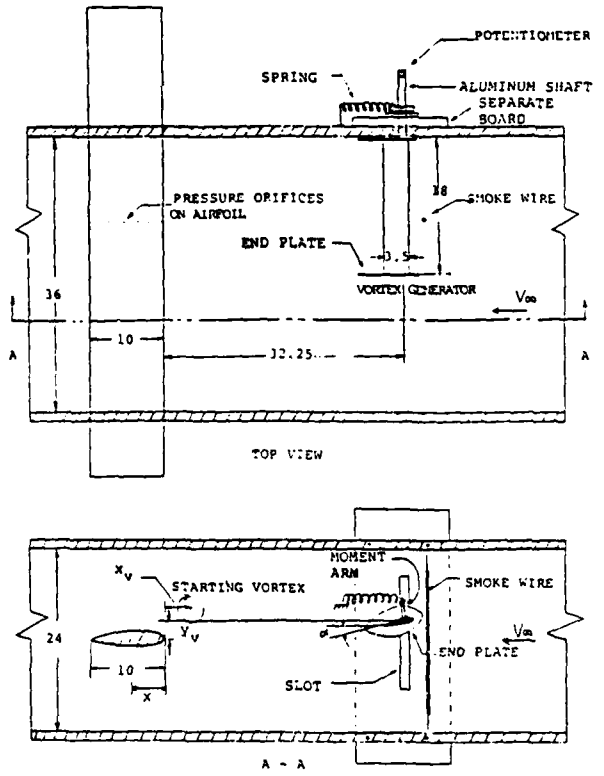

Fig. 4. UTA Low-Speed Wind Tunnel Test Set-Up for Blade-Vortex Interaction Test (Dimensions in Inches)

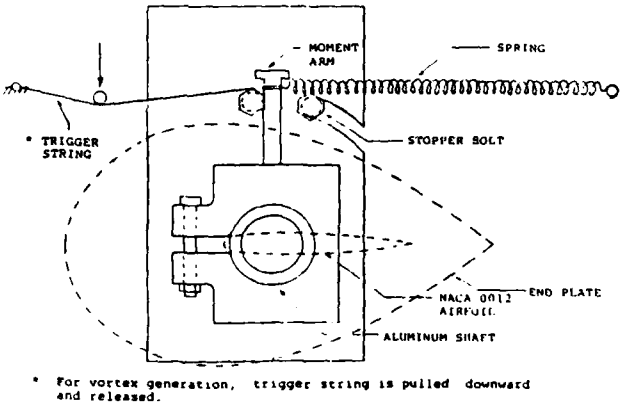

Fig. 5. Schematic Diagram of Vortex Generator

to a separate board outside the wind tunnel wall, which allowed the vortex generator to be moved in the vertical direction. A potentiometer was attached to the end of the shaft to measure pitch angle of the vortex generator.

Downstream of the vortex generator wing, a 6-foot-span, 10-inch-chord wing model (NACA 64A015 section) was mounted across the wind tunnel with both ends extending through wing-section-shaped holes in the side walls (see Fig. 4).This mechanism allowed the wing to be moved in the spanwise direction in order to position chordwise pressure taps installed on the upper and lower surfaces of the wing and connected to 1/16-inch-diameter (I.D.) vinyl tubes extended to outside the wind tunnel.

Pressure measurememts on the wing surface were made using a capacitance pressure transducer (SETRA Model 261, 1-psid range) connected to a 48-channel Scanivalve. This pressure tranducer was calibrated using an alcohol manometer for a reference pressure source. Pressure and pitch angle measurements were recorded on a oscillograph (Honeywell Visicorder Oscillograph Model 906C). Because only two channels were available on the oscillograph, only one pressure tap at a time was recorded (for each vortex generated) along with the generator pitch angle. Then another pressure tap was connected to the recorder and the test repeated. The pitch angle data were used to correlate time among the various tests. The data acquisition system is shown in Fig. 6.

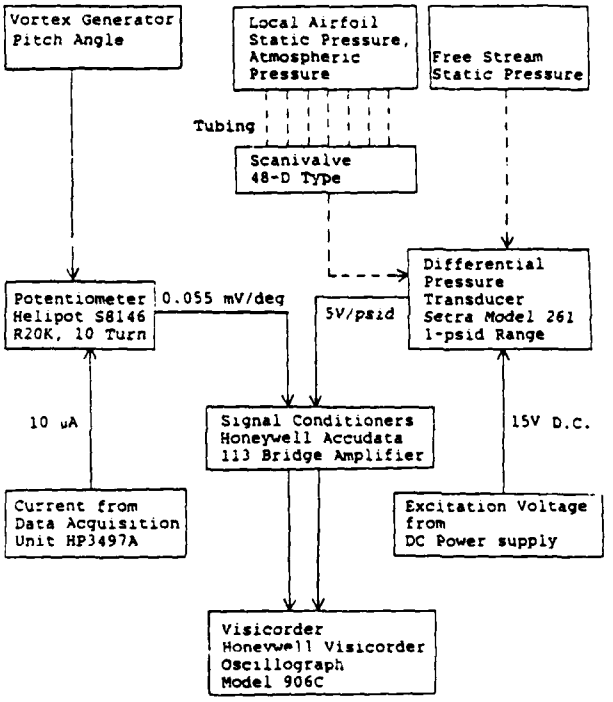

Fig. 6. Data Acquisition System

A smoke wire was placed across the test section upstream of the vortex generator, normal to the spanwise direction and to the free stream flow direction as shown in Fig. 4. Both ends of the smoke wire were connected to a variac which controled the input voltage to the smoke wire. The smoke was illuminated by a 120-volt, 1000-watt flood lamp located downstream of the tunnel diffuser. In order to observe the generation and movement of the vortex, a 16-mm high-speed (64 frames/sec) movie camera(Bolex H16 RX-5) loaded with an Eastman Ektakrome Tungsten film was utilized.

For the pressure tests, the free stream velociy was set at approximately 20, 30 and 40 ft/sec to obtain different reduced frequencies (reduced frequency, $k = \omega c_{v.g.}/V_\infty$). The vortex generator position was varied vertically with 1-inch increments and the maximum pitch angle was set at 10, 15 and 20 degrees. Right after the Visicorder

drive was turned on, the vortex was generated by impulsive pitching. While the vortex passed over the instrumented wing, the surface pressure and the pitch angle were recorded on the Visicorder paper. The pressure source was switched manually with the Scanivalve to the next position and the procedure was repeated.

The chordwise vortex position was calculated from the time history data of pressures with an assumption that the maximum wing surface pressure change at 1.25 % chord occurs when the center of the parallel vortex passes over the 1.25 % chord position. Another assumption was that the convection velocity of the vortex is equal to the free stream velocity. With these two assumptions, the time axis was rescaled to the chordwise passage of the vortex.

RESULTS AND DISCUSSION

For the flow visualization tests, the wind tunnel free stream velocity was set at 3 ft/sec in order to generate dense smoke and allow good quality of photographs. The temperature of the smoke wire was controlled by a variac. After the smoke was properly generated, the vortex generator was impulsively pitched from zero to a positive angle of attack to produce the parallel vortex. The generation and convection of the vortex were effectively recorded using the high-speed movie camera.

During the flow visualization tests, the 3 ft/sec of free stream velocity was calculated from the results of the high speed movie pictures. The reduced frequency(k = 0.8) was calculated from the free stream velocity above and the pitch rate which also was estimated from the high-speed movie pictures.

Sequential pictures of the flow visualization of the vortex generator were copied from the high-speed movie film. This movie included two types of pitch motion; a pitch-up-and-down motion and a pitch-up-and-hold motion. One end plate was removed to allow better viewing during movies.

A series of pictures in Fig. 7 shows the pitch-up-and-down motion of the airfoil. At initial position, no vortex can be seen (Fig. 7a) but when the pitch angle is approximately 26 degrees, the dynamic-stall vortex starts to form near the leading edge due to abrupt separation (Fig. 7b). At this time, the starting vortex has already formed near the trailing edge. The dynamic-stall vortex grows as pitch angle increases up to 45 degrees (Fig.7c),and sheds downstream (Fig. 7d). The starting vortex keeps traveling downstream (Figs.7c-7f). When the pitch angle returns to zero, the dynamic-stall vortex convects along the chord (Fig.7e) and leaves the trailing edge, but a stopping vortex was not observed as a separated vortex. Immediately after the dynamic-stall vortex leaves the airfoil, the starting vortex and the dynamic-stall vortex affect each other by inducing a downward motion and diffuse faster than in the case of a single starting vortex (Fig. 7f). A pair of vortices in pitch-up-and-down motion is not appropriate for a two-dimensional blade-vortex interaction simulation.

Another pitch motion was visualized with smoke (Fig. 8). The airfoil is pitched up from an initial position (Fig. 8a). After the pitching motion stopped at a low pitch angle, a starting vortex formed and shed downstream (Fig. 8f). At this low incidence angle a dynamic-stall vortex is not observed.

A well-defined vortex filament was generated by the pitch-up-and-hold motion. Therefore this technique was used in the following pressure tests of blade-vortex interaction.

Time histories of wing surface pressures are the basic data in the pressure tests. The effects of vortex height, reduced frequency, and maximum vortex generator angle, on the wing surface pressure are investigated.

Figures 9-11 show the time history of chordwise pressure distribution on upper and lower surfaces as the vortex passes over the wing. The free stream velocity was set at approximately 20 ft/sec and the reduced frequency k was calculated from the definition, $k = \dot{\alpha} C_{v.g.}/V_{\infty}$, where the pitch rate $\dot{\alpha}$ was estimated from the pitch angle data. A sample calculation of the pitch rate and the reduced frequency is shown in Fig. 12. In Figs. 9-11 the time axis was rescaled to the longitudinal vortex location with an assumption that the minimum of pressure at x/c = .0125 occurred when the vortex center passed over it. At the same time the convection velocity of the vortex was assumed to be equal to the free stream velocity. These figures show that the vortex-induced pressure on the upper surface decreases since the rotational direction of the starting vortex tends to increase the local velocity by an upwash effect. In the same way, the pressure rise on the lower surface can be explained in that the starting vortex induces a local velocity decrease. Severe pressure changes are seen near the leading edge at x/c = 0.0125 on upper and lower surfaces. The pressure changes become smaller from approximately x/c = 0.2 to the trailing edge. It is shown that the wing surface pressure starts to be influenced by the vortex when it passes upstream of the leading edge near x/c = -1, and the effect becomes insignificant when it passes two chord length downstream from the trailing edge (at x/c = 3). The discrepancy between the initial and final steady pressure in Figs. 9-Fig. 11 is primarily a result of the downwash induced by the pitched-up vortex generator's bound and trailing vortex system.

Figure 13 shows the effect of vortex proximity to the blade on the wing surface pressure at x/c = 0.0125. The time history of pressure at different vortex heights is presented. With an increase in blade-vortex separation, the amount of upwash induced by the vortex is decreased because circumferential velocity falls off with an increase in distance from the vortex center. The decreased upwash reduces the pressure changes on the upper and lower surfaces.

Time history of differential pressure at x/c = 0.0125 is depicted in Fig. 14, where the pressure was measured while varying the freestream velocity from 20 to 40 ft/sec.

The effect of vortex generator reduced frequency on the maximum pressure change at different locations of pressure taps is presented in Fig. 15. The maximum pressure change increases as the reduced frequency increases over the range tested.

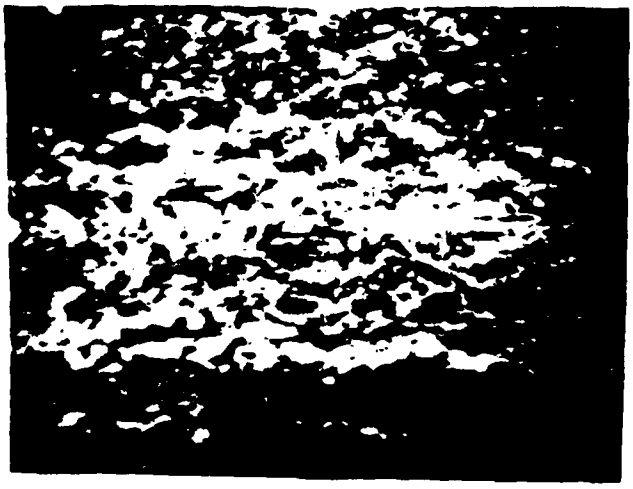

(a) initial position (α = 0 deg, T = 0 sec)

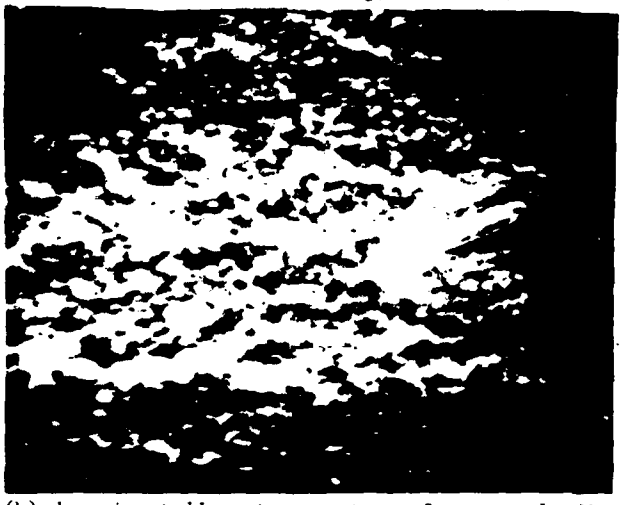

(b) dynamic-stall vortex starts to form near leading edge, starting vortex formed near trailing edge (α = 26 deg, T = 3/64 sec)

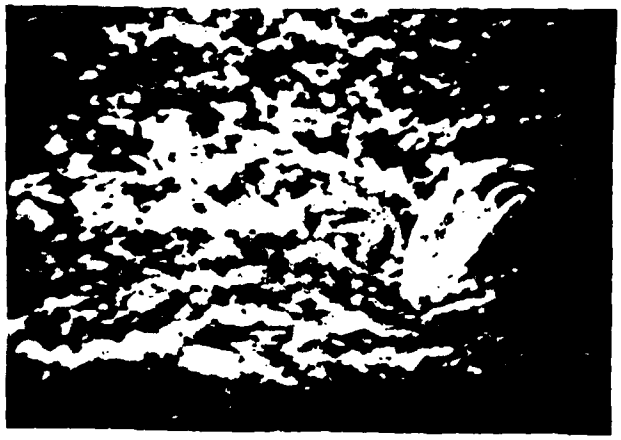

(c) starting vortex is shedding downstream and dynamic-stall vortex is growing (α = 45 deg, T = 6/64 sec)

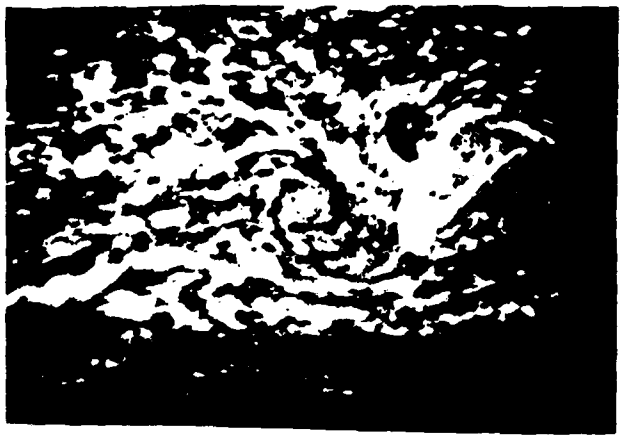

(d) dynamic-stall vortex is starting to shed (α = 42deg, T = 10/64 sec)

(e) dynamic-stall vortex is moving along the chord (α = 0 deg, T = 13/64 sec)

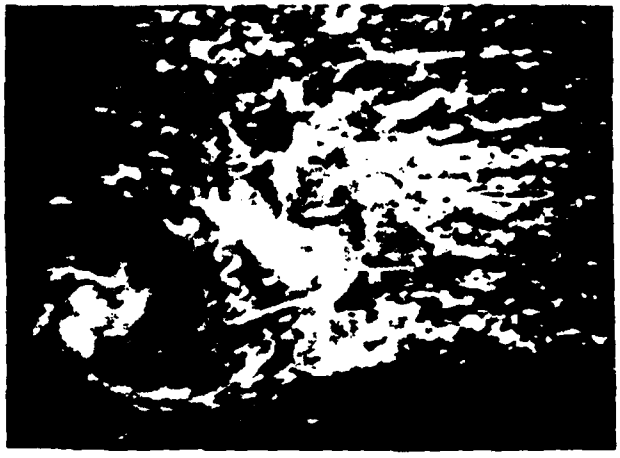

(f) dynamic-stall vortex and starting vortex induce downward motion and diffuse (α = 0 deg, T = 23/64 sec)

Fig. 7. Smoke Flow Visualization of Pitch-Up-and-Down Motion of Vortex Generator

(a) initial position (α = 0 deg, T = 0 sec)

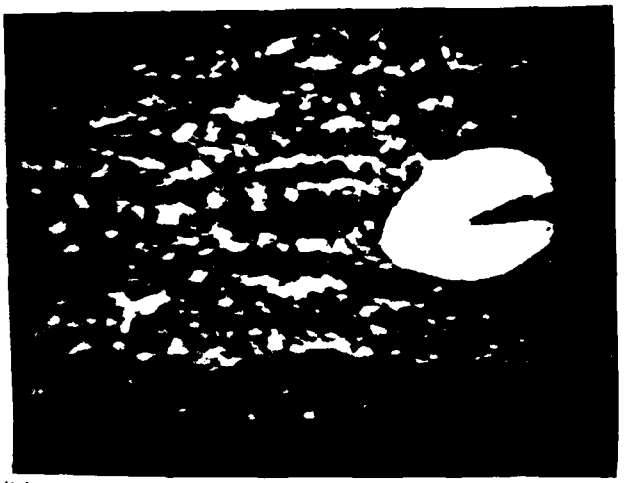

(b) starting vortex appears near the trailing edge of end plate (α = 15 deg, T = 5/64 sec)

(c) (α = 15 deg, T = 8/64 sec)

(d) (α = 15 deg, T = 14/64 sec)

(e) (α = 15 deg, T = 20/64 sec)

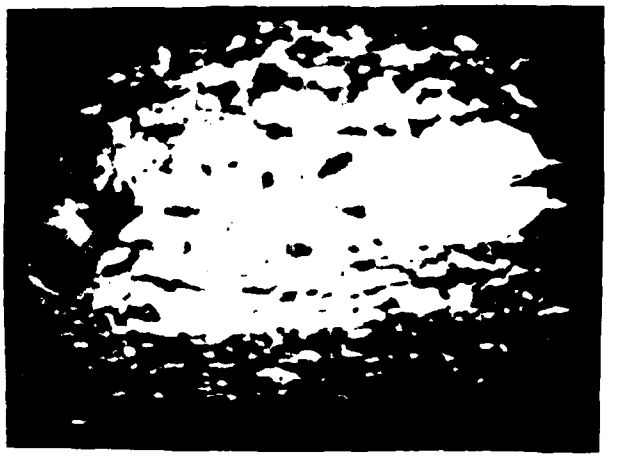

(f) (α = 15 deg, T = 23/64 sec)

Fig. 8. Smoke Flow Visualization of Pitch-Up-and-Hold Motion of Vortex Generator

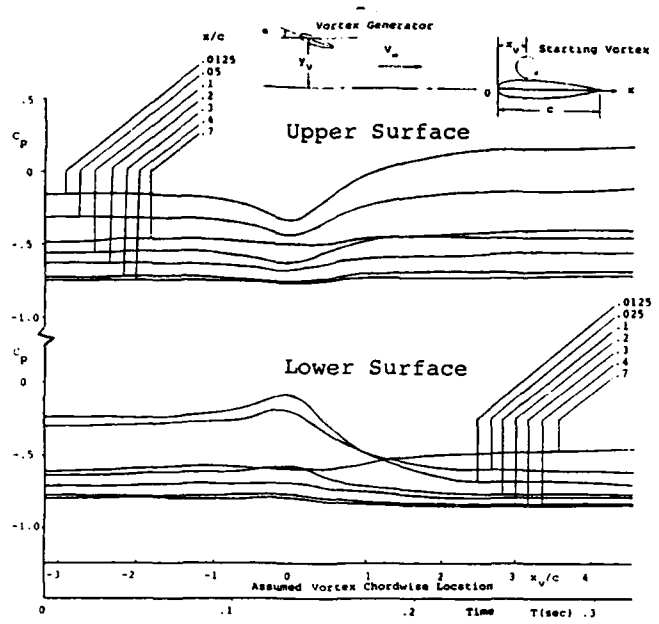

Fig. 9. Time History of Pressure Coefficient. V_∞ = 20 ft/sec, α_{max} = 10 deg, k = 0.55, y_v/c = 0.18.

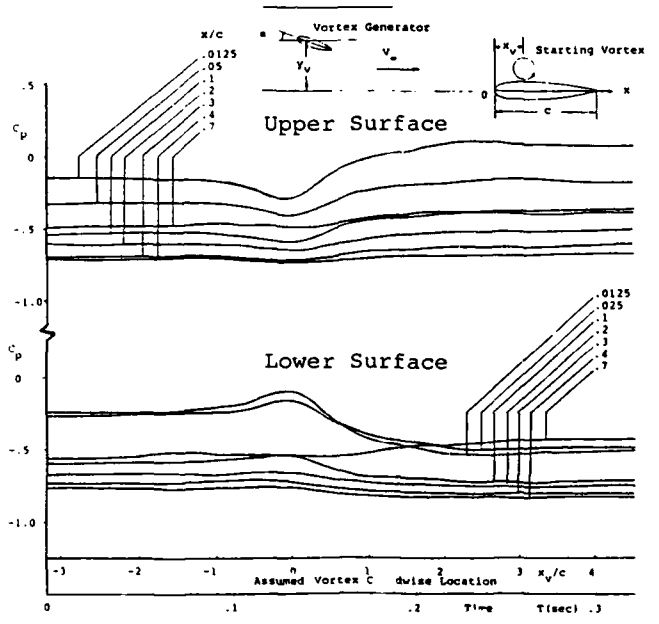

Fig. 10. Time History of Pressure Coefficient V_∞ = 20 ft/sec, α_{max} = 10 deg, k = 0.55, y_v/c = 0.28

The effect of vortex generator maximum pitch angle on the time history of pressures at two chordwise stations is shown in Fig. 16. Higher pitch angles induced larger pressure changes because a higher pitch angle produces a larger circulation in the starting vortex. As far as resultant forces are concerned, the bound vortex of proper strength in a uniform stream is equivalent to a body with

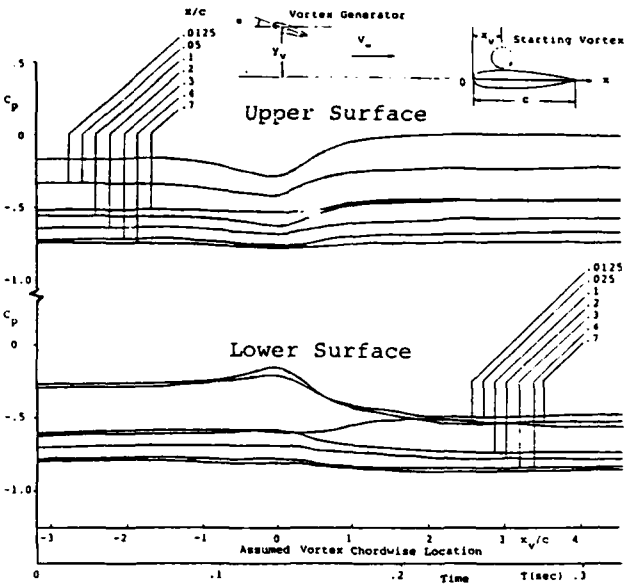

Fig. 11. Time History of Pressure Coefficient. V_∞ = 20 ft/sec, α_{max} = 10 deg, k = 0.55, y_v/c =0.38

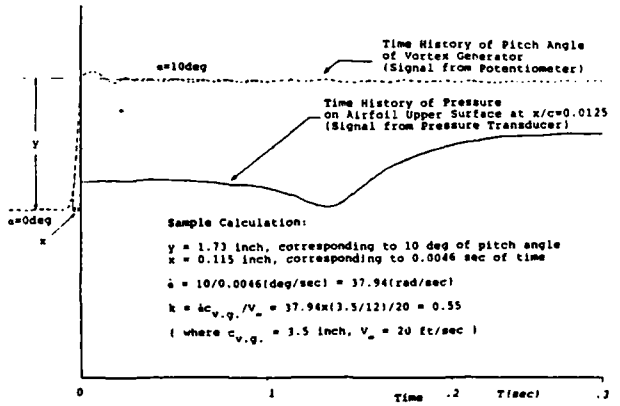

Fig. 12. Time History of Pitch Angle and Pressure, and Sample Calculation of Pitch Rate and Reduced Frequency

circulation in a uniform stream. Hence the vortex strength Γ can be related to lift coefficient as follows.

Section lift = $0.5\ \rho\ V_\infty^2\ c_{v.g.} C_\ell = \rho V_\infty \Gamma$. Then the vortex strength is

$$\Gamma = 0.5\ C_\ell V c_{v.g.}$$

The section lift coefficient for an NACA 0012 airfoil is obtained from Ref. 13. For the condition of dynamic stall, the airfoil passes the static-stall angle without significant change in lift-curve slope as can be seen in Ref. 14. Therefore the lift coefficient at an angle which is higher than the static-stall angle can be determined by linear extrapolation. Then the vortex strength of the vortex generator is estimated as follows

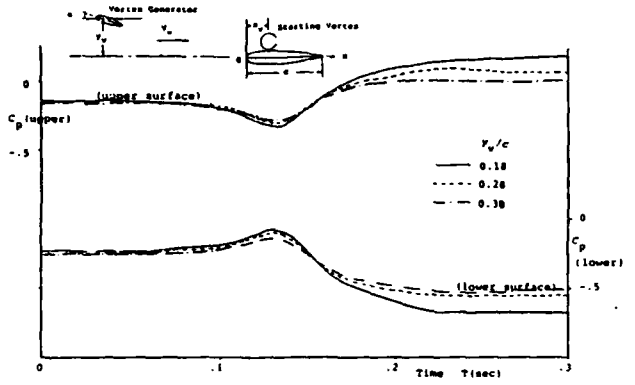

Fig. 13. Time History of C_p at x/c = 0.0125 as a Function of Vortex Height: V_∞ = 20 ft/sec, α_{max} = 10 deg, k = 0.55

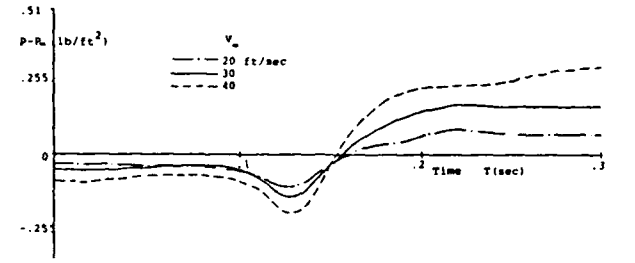

Fig. 14. Time History of Differential Pressure at x/c = 0.0125 as a Function of Free Stream Velocity: α_{max} = 10 deg, α = 37.94 rad/sec, y_v/c = 0.28, Upper Surface.

α(deg)	C_ℓ	Γ(ft^2/sec)
10	1.10	3.20
15	1.65	4.81
20	2.20	6.42

(V_∞ = 20 ft/sec, C_{vg} =3.5 in.)

This vortex strength appears to be related to the vortex induced pressure change as shown in Fig. 17. At higher pitch angles (15-20 deg), a maximum pressure was observed after the pressure experiences a minimum value (see Fig. 16). This appears to be due to the dynamic-stall vortex passing the instrumented wing after the starting vortex. Recalling that the rotational direction of the dynamic-stall vortex is opposite to that of the starting vortex, the dynamic-stall vortex induces a downwash effect opposite to the starting vortex's upwash effect. After the vortices passed downstream, more pressure fluctuations were observed at higher pitch angles. This is probably due to the flow separation wake from the vortex generator at the high pitch angles.

Figure 18 shows the time history of pressure for two different lengths of tube connected between the orifice and the pressure transducer. The 12-ft-long tube reduces the pressure change up to 60% and also delays the minimum pressure point by 0.016 sec compared with the 3-ft-long tube.

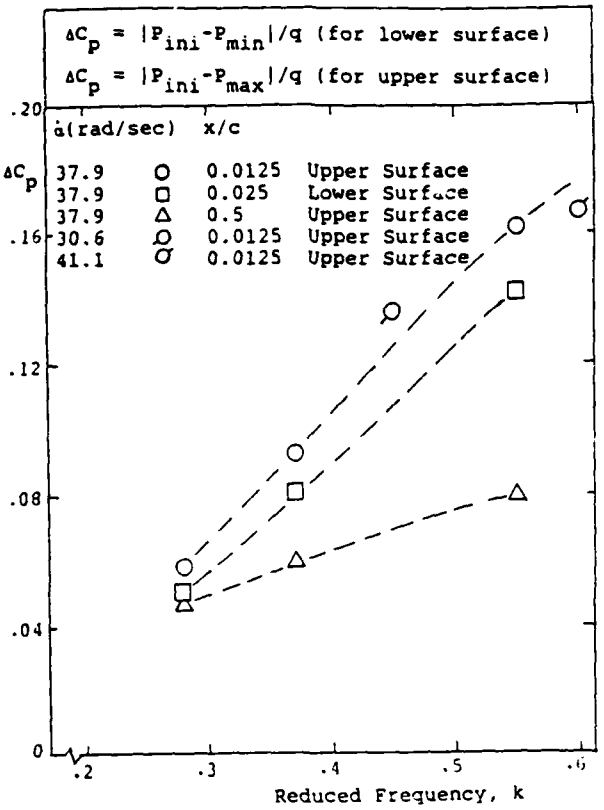

Fig. 15. Vortex-Induced Pressure Change vs Reduced Frequency of Vortex Generator.

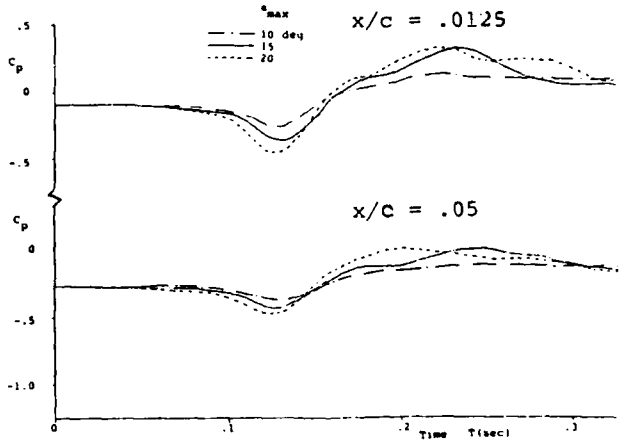

Fig. 16. Time History of C_p at x/c = 0.0125 (upper) and x/c = 0.05 (lower) as a Function of Maximum Pitch Angle of Vortex Generator: V_∞ = 20 ft/sec, k = 0.55, y_v/c = 0.28, Upper Surface.

CONCLUSIONS

A parallel vortex was generated from an impulsively-pitched wing in a low-speed wind tunnel. Smoke flow visualization revealed that a well-defined starting vortex was generated when the wing

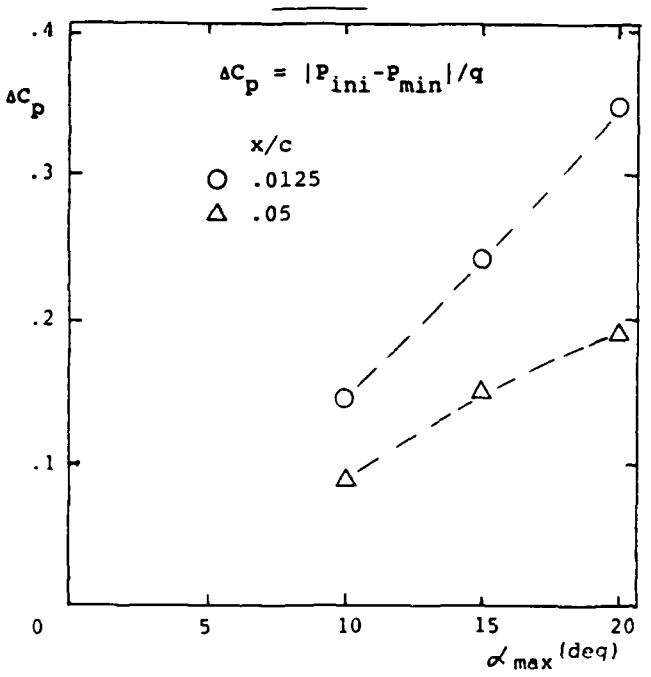

Fig. 17. Vortex-Induced Pressure Change vs Maximum Pitch Angle of Vortex Generator: V_∞ = 20 ft/sec, k = 0.55, y_v/c = 0.28, Upper Surface

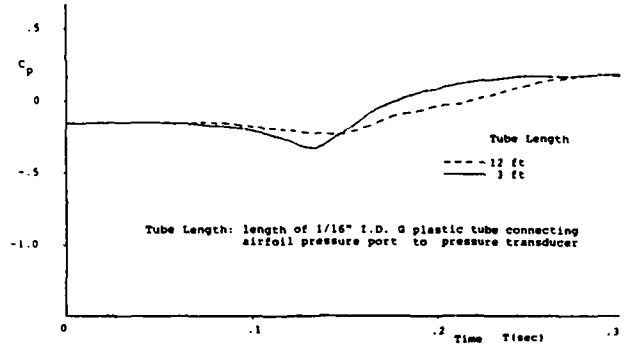

Fig. 18. Time History of C_p for Different Tube Lengths: V_∞ = 20 ft/sec, α_{max} = 10 deg, k = 0.55, y_v/c =0.18, x/c = 0.0125, Upper Surface

was stopped at a pitch angle of approximately 10 degrees.

Blade-vortex encounters were measured with a pressure transducer successively connected to the pressure orifices on the downstream airfoil. Time histories of pressures were recorded for a range of free stream velocities, vortex positions, maximum pitch angles of vortex generator and reduced frequencies.

Transient pressure changes (pressure rise on upper surface, pressure drop on lower surface) were measured as the vortex passed over the wing. This vortex-induced change is dominant near leading edge. This effect starts when the vortex passes approximately a chord length ahead of the wing and lasts until it passes two chord lengths aft of the trailing edge.

For the range of vortex heights tested, the tests showed that the pressure change increased as the vortex height decreased (passed closer to the wing).

The test data also show that the pressure change near the leading edge increased linearly as the reduced frequency of a vortex generator increased over the range of 0.28-0.55. It indicated that a higher reduced frequency produced a stronger vortex which, in turn, produced a larger pressure change near the leading edge of the wing.

The effect of maximum vortex generator pitch angle on the downstream wing surface pressure change increased as the pitch angle increased from 10 to 20 degrees. At the higher pitch angles (15 and 20 deg), a maximum pressure occurred after the pressure experiences a minimum value, which may be caused by a dynamic-stall vortex passing the instrumented wing after the starting vortex. Pressure fluctuations also increase after the vortex travels far downstream. This is probably due to the vortex generator flow separation wake.

Further shortening of the tube length connecting the pressure orifices to the pressure transducer would substantially reduce the response time and improve the accuracy of the quantitative data.

ACKNOWLEDGEMENTS

This work was supported by a grant from the Army Research Office, Contract DAAG29-84-K-0131, Experimental Simulation of Transonic Vortex-Airfoil Interactions, Dr. Thomas L. Doligalski, contract monitor. Scientific Liaison officer is Dr. Henry Jones at the Army Aeroflightdynamics Lab at Moffet Field, California.

REFERENCES

1. Sanford, D., "Panel Discussion at Workshop on Blade-Vortex Interactions", Ames Research Center, 1984.
2. George, A.R., "Helicopter Noise:State-of-the-Art", Journal of Aircraft, Vol.15, No.11, 1978.
3. Schmitz, F. H., Boxwell, D. A., Lewy, S. and Dahan, C., " Model-to-Full-Scale Comparisons of Helicopter Blade-Vortex Interaction Noise", Journal of American Helicopter Society, Vol.29, No.2, 1984.
4. Caradona, F. X., Laub, G. H. and Tung, C.,"An Experimental Investigation of the Parallel Blade-Vortex Interaction",Presented at Workshop on Blade-Vortex Interaction, Ames Research Center, 1984.
5. Surendriah, M.,"An Experimental Study of Rotor Blade-Vortex Interaction", NASA CR-1573, 1969.
6. Stepniewski, W. Z., Rotary-Wing Aerodynamics, Dover Publications, 1984.
7. Lugt, H. J., Vortex Flow in Nature and Technology, John Wiley & Sons, 1983.
8. Pruyn, R. R., "USAALABS Tandem Rotor Airloads Measurement Program", Journal of Aircraft, Vol. 4, No.3, 1967.
9. Widnall, S. E., "Helicopter Noise Due to Blade-Vortex Interaction", Journal of Acoustics Society of America, Vol.50, No. 1, 1970.

10. Widnall, S. E., "Effect of Tip Vortex Structure on Helicopter Noise Due to Blade-Vortex Interaction", Journal of Aircraft, Vol. 17, No. 10, 1980.
11. Kim, J.-M., "An Investigation of the Parallel Blade-Vortex Interaciton in a Low-Speed Wind Tunnel," M.S. Thesis, Univ. of Texas at Arlington, 1986.
12. Booth, E. R. and Yu, J. C., "Two Dimensional Blade-Vortex Interaction Flow Visualization Investigation", AIAA-84-2307, Presented at AIAA/NASA 9th Aeroacoustics Conference, Williamsburg, Virginia, October 15-17, 1984.
13. Abbott, I. H. and von Doenhoff, A. E., Theory of Wing Sections, Dover Publications, Inc., 1959.
14. McCroskey, W.J., Carr, L.W. and McAlister,K.W., "Analysis of the Development of Dynamic Stall based on Oscillating Airfoil Experiments", NASA TN D-8382, 1977.

between the wing bending vibration and the short period oscillation of the aircraft.

Acknowledgment

The author is grateful to Ken Griffin at Cranfield Institute of Technology for many useful discussions. He also wishes to thank his wife, Mala, for sustained encouragement.

References

[1]Banerjee, J. R., "Flutter Characteristics of High Aspect Ratio Tailless Aircraft," *Journal of Aircraft*, Vol. 21, Sept. 1984, pp. 733-736.

[2]Theodorsen, T., "General Theory of Aerodynamic Instability and Mechanisms of Flutter," NACA TR- 496, 1934.

Spanwise Displacement of a Line Vortex Above a Wing – A Simple Calculation Scheme

Yunggui Jung* and Donald D. Seath†
University of Texas at Arlington, Arlington, Texas

I. Introduction

WHEN a wing encounters a concentrated tip vortex, its aerodynamic characteristics are substantially altered due to nonlinear interaction. While the vortex affects the wing loads, the wing in turn affects the vortex path through its vorticity field.

Hancock[1] noticed the displacement of a streamwise line vortex over a two-dimensional wing and gave analytic expression for the sidewash velocity induced on the vortex by the wing trailing vorticity. Experimental evidence of this type of vortex motion was reported by Patel and Hancock[2] in their flow visualization study. Vortex motion due to secondary separation was observed by Harvey and Perry[3] in their investigation of trailing vortices in the vicinity of the ground. Recently, the displacement of a tip vortex above a two-dimensional wing surface was carefully measured in a low-speed wind tunnel for various conditions by Seath and Wilson.[4]

Meanwhile, it was recognized on the computational side[5,6] that the originally straight vortex should be allowed to align itself with the local streamline direction in order to obtain a better solution to the vortex-wing interaction calculations.

It is generally believed that some kind of iteration scheme is necessary to account for the mutual influence between the vortex and the wing trailing vorticity and, thus, to obtain an acceptable vortex path and its effect on induced airloads. However, for the flow conditions considered in this paper, i.e., low subsonic speed, it is found that the detailed temporal variation of the wing trailing vortex sheet due to the deforming line vortex has little efect on the motion of the vortex line over the wing surface, and that the spanwise displacement of a line vortex can be calculated in a straightforward manner without iteration coupled with wake evolution.

The present method is based on the lifting line solution of the spanwise load distribution. A single lifting line cannot adequately represent a wing as far as the chordwise variation of the wing vorticity is concerned. However, a very simple trick of redistributing the calculated bound vorticity along the chord in accordance with the "thin airfoil theory" produces surprisingly good results.

II. Description of the Present Method

The model consists of an infinite line vortex, which is originaly parallel to the freestream, and a finite wing as shown in Fig. 1, together with the coordinate system.

Received Oct. 22, 1986; revision received Nov. 23, 1987.

*Graduate Teaching Assistant, Department of Aerospace Engineering.

†Professor, Department of Aerospace Engineering.

The velocity field induced by an infinite line vortex is given by the Biot-Savart law as

$$V_i(r)=\frac{\Gamma_o \times r}{2\pi r^2} \tag{1}$$

where V_i is the induced velocity, Γ_o the circulation of the line vortex, and r the radial vector from the vortex line to a field point. The induced angle of attack at any section along the span is obtained by taking the z-component of this induced velocity and dividing it by the freestream velocity. Thus for a vortex of height h

$$\alpha_i(y)=\frac{\Gamma_o}{2\pi V_\infty}\frac{y}{h^2+y^2} \tag{2}$$

where α_i is the induced angle of attack, and V_∞ the freestream velocity. If we regard this induced angle of attack as additional twist to the section angle of attack of the wing in a uniform freestream, we can calculate the spanwise variation of circulation by solving a modified lifting line equation[7]

$$\Gamma(y)=\frac{1}{2}a_o(y)c(y)\,V_\infty\Big[(\alpha_w+\alpha_i) - \frac{1}{4\pi V_\infty}\int_{-b/2}^{b/2}\frac{d\Gamma}{dy}(\eta)\frac{d\eta}{y-\eta}\Big] \tag{3}$$

Approximate solution to this equation can be obtained to any desired accuracy by a suitable iteration scheme combined with a numerical quadrature, e.g., Ref. 8.

Whereas $\Gamma(y)$ is usually associated with a lifting line located at the quarter-chord line of the wing, we can distribute the total circulation at any section along the chord so that we have as many lifting lines as we want. From the thin airfoil theory we know for a flat plate at an angle of attack α

$$\gamma(\theta)=2V_\infty\alpha\tan(\theta/2) \tag{4}$$

where γ is the vortex strength and θ is related to x by

$$x=(c/2)(1+\cos\theta)$$

If we have n sublifting lines to represent the airfoil chord, the strength of each line may be obtained by integrating Eq. (4). This gives

$$\Gamma_i=\frac{\Gamma}{\pi}[\theta-\sin\theta]_{\theta_{i-1}}^{\theta_i} \qquad i=1, 2, \ldots, n \tag{5}$$

where n is the total number of lifting lines along the chord.

Each of these lifting lines sheds a vortex sheet of strength $-d\Gamma_i/dy$ downstream. For simplicity, we may assume that all the vortex sheets remain undistorted and parallel to the freestream. Therefore, if the wing is at 0 deg incidence, all the vortex sheets will be in the $x=y$ plane. Then, the sidewash

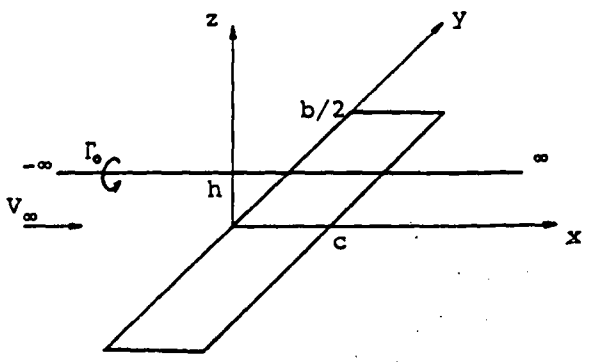

Fig. 1 Model and coordinate system.

velocity induced at a point on the vortex line by the ith trailing vortex sheet is

$$v_i(x,y,h) = \frac{h}{4\pi}\left(1 + \frac{|x-x_i|}{\sqrt{(x-x_i)^2+h^2}}\right) \int_{-b/2}^{b/2} \frac{d\Gamma}{dy}(\eta)\,\frac{d\eta}{h^2+(\eta-y)^2} \tag{6}$$

and the total sidewash at the same point is

$$v(x,y,h) = \sum_{i=1}^{n} v_i(x,y,h) \tag{7}$$

From this we can calculate the spanwise displacement of the vortex by time integration.

Convergence of the calculations is expected on the grounds that the influence of the vortex sheets on fluid particles located far upstream of the wing is negligible. Thus, some part of the free vortex does not move sideways.

As the vortex line deforms from its initial straight line, the induced airload will change accordingly. However, unless the free vortex is very close to the wing surface, we may further assume that this change is small for most of the wing. Then, we may freeze the trailing vortex sheets at the initial state. This means that we only need to compute the trailing vorticity due to the free vortex once and for all and do not have to update the wake field each time the free vortex assumes a new position. It turns out that this assumption is totally adequate for the test cases considered in the present paper.

III. Application and Discussion

The present method has been applied to a low subsonic vortex-airfoil interaction problem with very encouraging results. The input data were taken from the wind tunnel tests conducted at the University of Texas at Arlington by Seath and Wilson.[4] The test setup is shown in Fig. 2.

Specifically, the vortex strength $\Gamma_o/V_\infty c = 0.288$; wing span $b = 3$ ft; lift curve slope $a_o = 6.0$/rad; chord length $c = 10$ in.; vortex heights $h/c = 0.075$, 0.095, and 0.13. With these values, induced angles of attack were obtained, and the modified lifting line equation was solved via the numerical iteration scheme of Multhopp using 81 spanwise stations. The resulting circulation was then distributed along the chord into 10 sublifting lines located at $x/c = 0.05, 0.15, \ldots, 0.95$.

The results are shown in Figs. 3-5. As seen in these figures the agreement with the experimental data is quite striking when we recall that the wake of the wing was "frozen" at its initial state with no later update. Figure 6 shows vortex

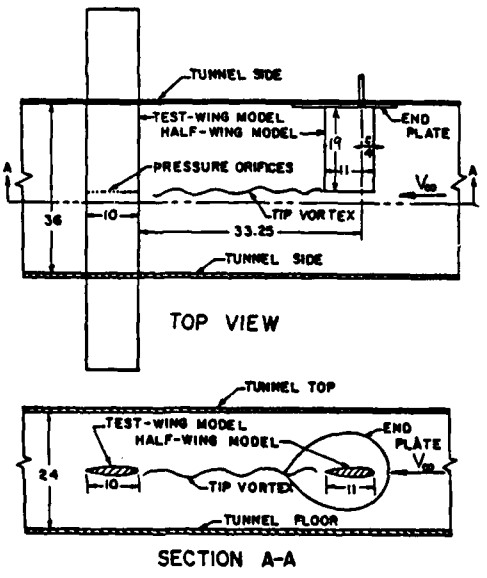

Fig. 2 Test setup.[4]

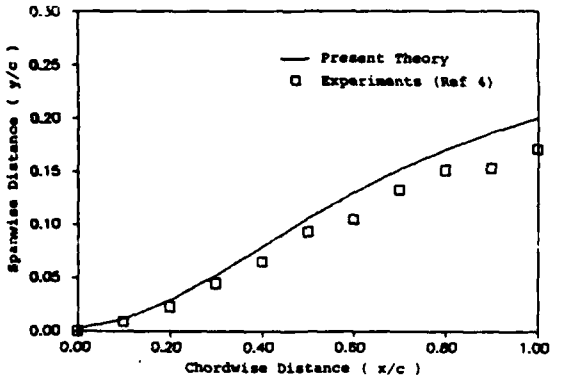

Fig. 3 Vortex path ($h/c = 7.5\%$, $\Gamma_o/V_\infty c = 0.288$).

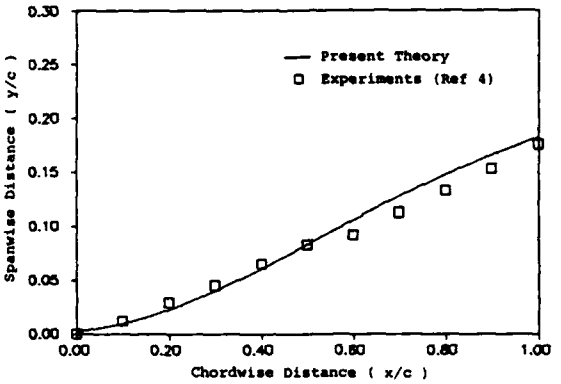

Fig. 4 Vortex path ($h/c = 9.5\%$, $\Gamma_o/V_\infty c = 0.288$).

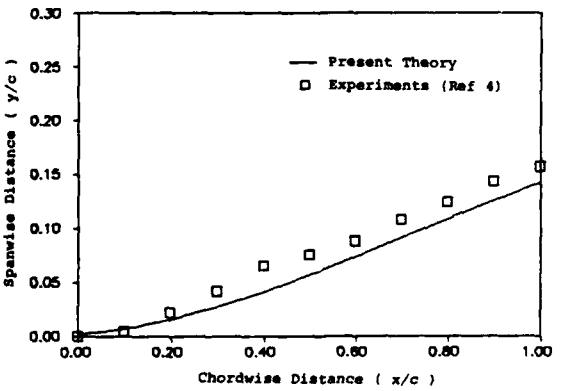

Fig. 5 Vortex path ($h/c = 13\%$, $\Gamma_o/V_\infty c = 0.288$).

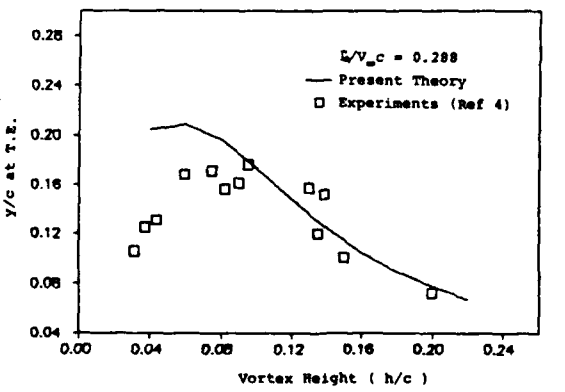

Fig. 6 Spanwise displacement vs height of vortex.

displacement at the wing trailing edge for various vortex heights. Here again, the present theory produces reasonable estimates. As is anticipated, however, a potential vortex model overpredicts the vortex effect in a very close encounter of vortex and wing due to its singularity at the center. This is evident in the figure by the deviation of the curve from the squares for h/c less than about 0.1. This situation may be improved by modeling a finite vortex core.

Overall, the results are very encouraging, and this suggests that the present method may be used as a preprocessor to prescribe the vortex path over a lifting surface for vortex-lifting surface interaction calculations within the restrictions of the potential flow assumptions. This will eliminate the need to assume a straight vortex and update the whole flow field as well as the vortex path. Or, in cases where complex configurations are involved, the present method may provide a reasonable starting position of the vortex for a coupled iteration scheme.

Acknowledgment

A portion of the work was performed under Army Research Office Contract DAAG 29-84-K-0131, Experimental Simulation of Transonic Vortex-Airfoil Interactions.

References

[1]Hancock, G. J., "Aerodynamic Loading Induced on a Two-Dimensional Wing by a Free Vortex in Incompressible Flow," *The Aeronautical Journal of the Royal Aeronautical Society*, Vol. 75, June 1971, pp. 413–416.

[2]Patel, M. H. and Hancock, G. J., "Some Experimental Results of the Effect of a Streamwise Vortex on a Two-Dimensional Wing," *Aeronautical Journal*, April 1974, pp. 151–155.

[3]Harvey, J. K. and Perry, F. J., "Flowfield Produced by Trailing Vortices in the Vicinity of the Ground," *AIAA Journal*, Vol. 9, Aug. 1971, pp. 1659–1660.

[4]Seath D. D. and Wilson, D. R., "Vortex-Airfoil Interaction Tests," AIAA Paper 86-0354, Jan. 1986.

[5]Maskew, B., "Predicting Aerodynamic Characteristics of Vortical Flows on Three-Dimensional Configurations Using a Surface-Singularity Panel Method," AGARD-CP-342, 1983.

[6]Steinhoff, J., Ramachandran, K., and Suryanarayanan, K., "The Treatment of Convected Vortices in Compressible Potential Flow," AGARD-CP-342, April 1983.

[7]Karamcheti, K., *Principles of Ideal-Fluid Aerodynamics*, John Wiley, New York, 1966, Chap. 19, pp. 538–545.

[8]Bisplinghoff, R. L., Ashley, H., and Halfman, R. L., *Aeroelasticity*, Addison-Wesley, Reading, Mass., 1955, Chap. 5, pp. 231–237.

Divergence Study of a High-Aspect-Ratio, Forward Swept Wing

Stanley R. Cole*

NASA Langley Research Center, Hampton, Virginia

Introduction

THE present study was conducted to obtain data that could be used to assess the prediction capabilities of a currently available aeroelastic code for a high-aspect-ratio, forward-swept wing. A wind tunnel experiment was conducted in the NASA Langley Transonic Dynamics Tunnel (TDT) on a model with a panel aspect ratio of 9.16 (unswept). Aeroelastic analyses were conducted for each condition tested in the TDT for this comparison. The wind tunnel model was tested at various forward sweep angles. A rectangular tip shape was used during most of the experiment. A tip parallel to the flow in the 45 deg forward-sweep position was also tested for further correlation with analysis. General aeroelastic characteristics of the high-aspect-ratio, highly swept wing, and the prediction capabilities of the analysis code are discussed in this Note.

Presented as Paper 86-0009 at the AIAA 24th Aerospace Sciences Meeting, Reno, NV, Jan. 6–9, 1986; received Feb. 2, 1986; revision received Nov. 23, 1987.

*Aerospace Technologist, Configuration Aeroelasticity Branch. Senior Member AIAA.

Test Apparatus and Procedures

The model used in this study was untapered, had a 4.51 ft semispan and a semispan aspect ratio of 9.16 in the unswept position. The airfoil section was a NACA 0014. The model wing was constructed of a layered fiberglass shell, which provided both structural stiffness and the airfoil shape, with a rectangular aluminum spar located at the 30% chord position to increase the bending stiffness. Semicircular wing tips made of balsa wood were used to improve the flow over what would otherwise have been a blunt wing tip in the forward-sweep positions. The model was clamped in a cantilevered manner to the wind-tunnel sidewall.

The model was positioned manually to sweep angles Λ of 0, -15, -30, -45 and -60 deg. A composite photograph showing the model in the various sweep angles is shown in Fig. 1. The model was tested with a rectangular wing tip at each azimuth angle as shown in the figure. In addition, the wing tip was modified such that the tip was parallel to the freestream flow when tested in the $\Lambda = -45$ deg position. The two tip shapes are shown in Fig. 1 at $\Lambda = -45$ deg.

Experimental predictions of static aeroelastic divergence were made using subcritical response techniques.[1] For each sweep angle tested, subcritical data were taken at gradually increasing values of dynamic pressure. At each dynamic pressure q, the model angle of attack was first adjusted to a 1-g lift condition so that the weight of the model was aerodynamically supported. The angle of attack was then incrementally increased and the root bending moment M_e was measured at each angle of attack α. Typical data obtained for the subcritical response divergence predictions are shown in Fig. 2. These data were used to predict the dynamic pressure at which divergence would occur. Two subcritical response techniques, an improved static Southwell method and the divergence index method, were used during this test. Reference 1 discusses these prediction methods in greater detail.

Analytical Tools

Aeroelastic analyses were conducted for the wind-tunnel model to determine the validity of the analysis code for a high-aspect-ratio, highly swept wing. A vibration analysis was performed with the finite-element method program[2] Engineering Analysis Language (EAL). General beam elements were utilized to assemble the finite-element model. Elements were ar-

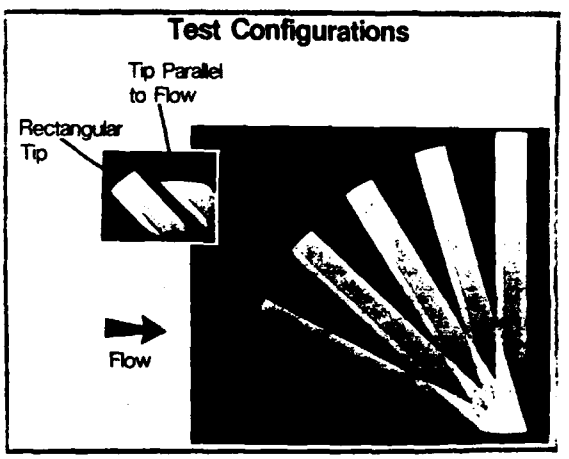

Fig. 1. Composite photograph showing each sweep angle tested and the two tip shapes tested in the $\Lambda = -45$ deg configuration.

INVESTIGATION OF THE PARALLEL BLADE-VORTEX INTERACTION AT LOW SPEED

D. D. Seath*, Jai-Moo Kim** and D. R. Wilson*
The University of Texas at Arlington
Arlington, Texas 76019

ABSTRACT

Low-speed wind tunnel tests were conducted to investigate the parallel blade-vortex interaction. Flow visualization tests of vortex generation performed prior to the pressure tests showed that a well-defined starting vortex was generated by an implusively pitched wing. Time history of the pressure distribution on a pressure-tapped wing model was acquired as the starting vortex passed over the wing. These pressure tests revealed that a substantial pressure change near the leading edge was induced by the encountering vortex. The effects of vortex proximity, reduced frequency and maximum pitch angle of the vortex generator on the pressure change were also investigated.

---

* Professor of Aerospace Engineering

** Graduate Research Assistant, AE Department

ABSTRACT OF PAPER ACCEPTED FOR PUBLICATION
IN AIAA JOURNAL OF AIRCRAFT

AN EXPERIMENTAL INVESTIGATION OF THE PARALLEL VORTEX-AIRFOIL INTERACTION AT TRANSONIC SPEEDS*

Donald R. Wilson+, Iraj M. Kalkhoran++, and Donald D. Seath+
The University of Texas at Arlington
Arlington, Texas 76019

ABSTRACT

Unsteady vortex-airfoil interaction experiments at transonic Mach numbers ranging from 0.7-0.85, and airfoil chord Reynolds numbers of 3.5-5.5 million were conducted in the UTA high Reynolds number, transonic, Ludwieg-tube wind tunnel facility. The vortex-airfoil interaction experiments were designed to simulate a two-dimensional blade-vortex interaction (BVI) problem frequently encountered in rotorcraft applications. The interaction experiments involved positioning a two-dimensional vortex generator upstream of a NACA 0012 airfoil section and implusively pitching the vortex generator airfoil such that the starting vortex interacted with the downstream airfoil. Experiments were conducted at several vortex core heights above the downstream airfoil. The experimental results indicate a substantial change in the pressure distribution near the leading 30 percent of the interacting airfoil. Experimental data for supercritical Mach numbers indicated a very strong interaction of the vortex and the shock wave; and at closer encounters these interactions resulted in unsteady local flow separation of the leading 40 percent of the airfoil chord. Experiments with stronger vortices at supercritical Mach numbers resulted in a forward propagation of the shock wave.

---

*Work supported by ARO Grant DAAG29-84-K-0131, Dr. Tom Dolagalski, contract monitor.

+Professor, Aerospace Engineering Department, Associate Fellow, AIAA

++Visiting Assistant Professor, Aerospace Engineering Department, Member, AIAA

ABSTRACT OF PAPER BEING PREPARED FOR
PRESENTATION AT AIAA 20TH FLUID DYNAMICS,
PLASMADYNAMICS AND LASERS CONFERENCE,
BUFFALO, NY, JUNE 12-14, 1989